Carboniferous Highly Fractionated I-type Granites from the Kalamaili Fault Zone, Eastern Xinjiang, NW China: Petrogenesis and Tectonic Implications

SONG Peng[1], WANG Tao[1, 2, *], TONG Ying[1], ZHANG Jianjun[1], HUANG He[1], ZHANG Lei[1], QIN Qie[1] and SHEN Huan[3]

[1] *Key Laboratory of Deep-Earth Dynamics of Ministry of Natural Resources, Institute of Geology, Chinese Academy of Geological Sciences, Beijing 100037, China*
[2] *Beijing SHRIMP Center, Beijing 100037, China*
[3] *China Uuiversity of Geosciences, Beijing 100037, China*

Abstract: Carboniferous magmatism is one of the most important tectonothermal events in the Central Asian Orogenic Belt (CAOB). However, the final closure time of the Kalamaili Ocean between East Junggar and Harlik Mountain is still debated. Early Carboniferous (332 Ma) and late Carboniferous (307–298 Ma) granitic magmatism from Kalamaili fault zone have been recognized by LA-ICP-MS zircon U-Pb dating. They are both metaluminous highly fractionated I-type and belong to the high-K calc-alkaline. The granitoids for early Carboniferous have zircon $\varepsilon_{Hf}(t)$ values of −5.1 to +8.5 with Hf model ages (T_{DM2}) of 1.78–0.83Ga, suggesting a mixed magma source of juvenile material with old continental crust. Furthermore, those for late Carboniferous have much younger heterogeneous zircon $\varepsilon_{Hf}(t)$ values (+5.1 to +13.6) with Hf model ages (T_{DM2}=1.03–0.45 Ga) that are also indicative of juvenile components with a small involvement of old continental crust. Based on whole-rock geochemical and zircon isotopic features, these high-K granitoids were derived from melting of heterogeneous crustal sources or through mixing of old continental crust with juvenile components and minor AFC (assimilation and fractional crystallization). The juvenile components probably originated from underplated basaltic magmas in response to asthenospheric upwelling. These Carboniferous highly fractionated granites in the Kalamaili fault zone were probably emplaced in a post-collisional extensional setting and suggested vertical continental crustal growth in the southern CAOB, which is the same or like most granitoids in CAOB. This study provides new evidence for determining the post-accretionary evolution of the southern CAOB. In combination with data from other granitoids in these two terranes, the Early Carboniferous Heiguniangshan pluton represents the initial record of post-collisional environment, suggesting that the final collision between the East Junggar and Harlik Mountain might have occurred before 332 Ma.

Key words: highly fractionated granite, petrogenesis, carboniferous, Kalamaili fault zone, post-collisional magmatism

Citation: Song et al., 2019. Carboniferous Highly Fractionated I-type Granites from the Kalamaili Fault Zone, Eastern Xinjiang, NW China: Petrogenesis and Tectonic Implications. Acta Geologica Sinica (English Edition), 93(5): 1169–1187. DOI: 10.1111/1755-6724.14360

1 Introduction

The Altaids (e.g., Şengör et al., 1993; Xiao et al., 2008, 2009) or Central Asian Orogenic Belt (CAOB; e.g., Jahn et al., 2000a, b, 2004; Kovalenko et al., 2004; Windley et al., 2007), is a complex collage of microcontinental blocks, island arcs, oceanic crustal remnants and continental marginal facies rocks developed between the Siberia Craton to the north and the Tarim and North China cratons to the south. It is one of the largest and most complex Phanerozoic accretionary orogenic belts on Earth, recording considerable juvenile crustal growth (Şengör et al., 1993; Jahn et al., 2000a, b, 2004; Kovalenko et al., 2004; Windley et al., 2002, 2007; Cawood et al., 2009; Xiao et al., 2009; Wilhem et al., 2012; Li et al., 2013a).

The Late Paleozoic in the CAOB is characterized by tectonic transition and crustal growth with voluminous juvenile granitoids with positive Nd-Hf isotopic signatures (Han et al., 1997; Jahn et al., 2000a, 2004; Chen and Jahn, 2004; Yuan et al., 2007; Seltmann et al., 2011; Li et al., 2016). The Kalamaili fault is a very important geological boundary separated East Junggar from Harlik Mountain in North Xinjiang. It is a key area to understand the tectonic evolution of the southwestern CAOB (Xiao et al., 2010). Voluminous granitoids are located on both sides of the fault. Many studies have been carried out on the Carboniferous-Permian granitoids in this area (e.g. Han et al., 1997; Chen and Jahn, 2004; Liu et al., 2013). However, the geodynamical setting of the Carboniferous tectonothermal magmatism along the Kalamaili belt in the North Xinjiang has remained controversial, especially Carboniferous post-collisional/orogenic processes, including when it began and magma source, are still poorly constrained due to the scarcity of geochemical and geochronological data (e.g. Windley et al., 2007; Yuan et al., 2010; Yang et al., 2011).

* Corresponding author. E-mail: taowang@cags.ac.cn

Although a large number of studies have been done on granitoids from East Junggar and Harlik Mountain, these studies mainly focus on A-type granites. (e.g. Chen et al., 2004; Yuan et al., 2007; Yang et al., 2011). Now, much attention should be paid on the highly fractionated I-type granite. Accordingly, the precise age and petrogenesis of the Carboniferous granitoids can provide key evidence for constraining the tectonic transition of North Xinjiang. This paper shows new zircon U-Pb ages, whole-rock major and trace element compositions and Lu-Hf isotopic characteristics for Kalamaili granitic plutons, and discusses their petrogenesis, magma source and tectonic implications.

2 Geological Setting

The East Junggar and Harlik Mountain are important tectonic units of the southwestern part of CAOB, and are separated by the Kalamaili fault zone. The Kalamaili suture is in eastern North Xinjiang, China where the Kalamaili ophiolite crops out (Fig. 1). The ophiolite was interpreted as remnants of a Middle Paleozoic Kalamaili ocean which separates the Angaran plate to the north from the East Tianshan domain to the south (Xiao et al., 2004). Recent radiometric dating of plagiogranites and gabbros from the ophiolite yielded ages ranging from 417 to 330 Ma (Wang et al., 2009; Huang et al., 2012; Qin, 2012; Xu et al., 2015a). The rocks are structurally imbricated with strongly deformed Devonian-Carboniferous arc volcanic rocks. Volcanic and associated pyroclastic rocks, and turbidites, ranging from Ordovician-Silurian to Devonian-Early Carboniferous in age, of possible forearc basin origin were also imbricated into the accretionary wedge (Xiao et al., 2004).

2.1 East Junggar

East Junggar is bounded by the Kalamaili suture to the south and separated from the Chinese Altai Block to the north by the Erqis (or Irtysh) suture (Fig. 1, Sun et al., 2009; Long et al., 2012; Li et al., 2015, 2017). Tectonically, East Junggar has commonly been regarded as Paleozoic island arc in origin for its ubiquitous Paleozoic rock assemblages (e.g., Xiao et al., 2004; Long et al., 2012; Han et al., 2018). Gu et al. (1999) found that granitic rocks of calc-alkaline geochemistry, are distributed along the Kalamaili fault southeastwards to Harlik on both sides of the Kalamaili ophiolitic zone. It consists, from north to south, of the Dulate composite island arc, the Aermantai ophiolite mélange belt and the Yemaquan composite island arc. The Dulate arc is composed almost of Devonian island arc rocks, with a small amount of Ordovician limestone and some Carboniferous island arc volcanics (Xiao et al., 2004). The Yemaquan is mainly composed of Devonian volcano-sedimentary rocks, with some Ordovician-Carboniferous rocks and minor Jurassic sedimentary rocks. Granitoids in East Junggar were mostly emplaced in late Paleozoic, and mainly have zircon ages of 330–265 Ma, peaked at ca. 300 Ma (e.g., Han et al., 2006; Liu et al., 2013; Song et al., 2018). They are distributed cross important geological boundaries (such as an ophiolite zone, Han et al., 2006). The rock types are predominantly K-feldspar granite, granodiorite, monzogranite and alkaline granite, with A-type and I-type features (e.g. Liu et al., 2013). These granitoids have been formed in the post-collisional setting (e.g., Chen et al., 2004; Han, et al., 2010; Yang et al., 2011).

2.2 Harlik Mountain

The Harlik arc, which is located south of the Kalamaili

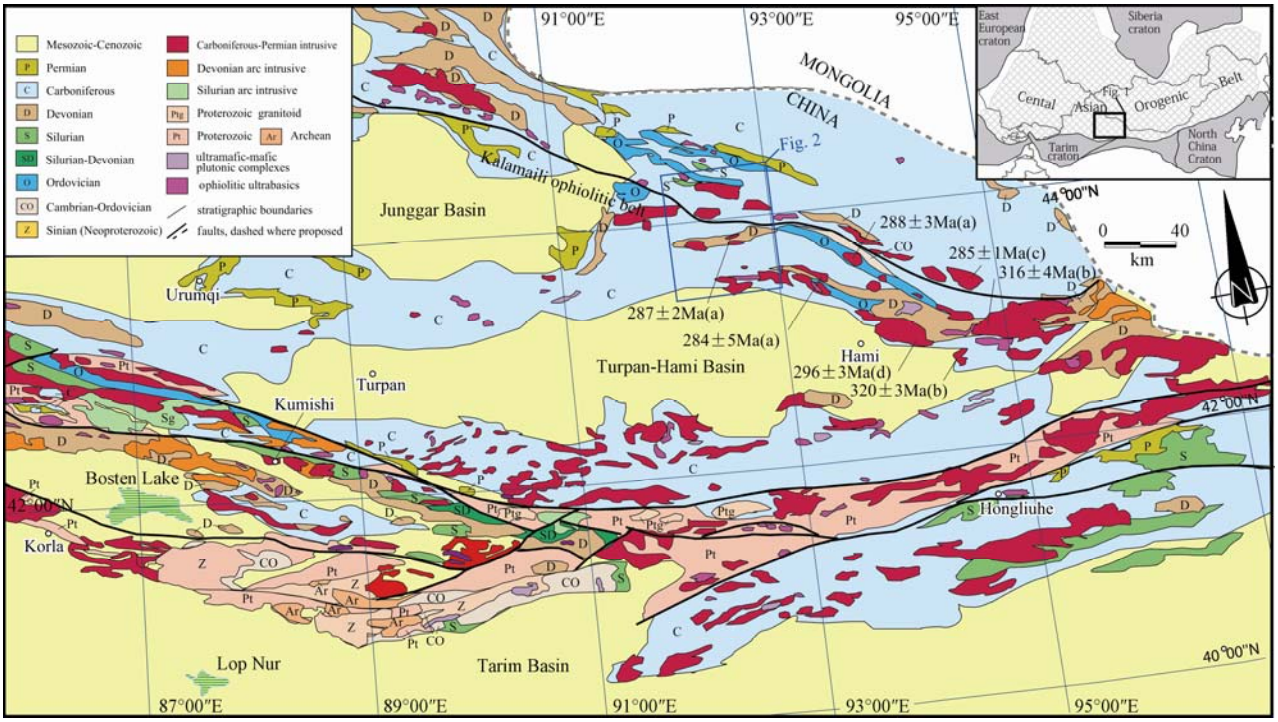

Fig. 1. Geological sketch map of East Xinjiang and granitoids distribution.
(after Xiao et al., 2004. Age data: (a)Yuan et al., 2010; (b) Song et al., 2018; (c) Wang et al., 2009; (d) Wang et al., 2010)

fault (Fig. 1), is a Paleozoic island arc, resulting from the consumption of the Kalamaili ocean basin. The oldest rocks are Lower Ordovician metamorphosed clastics, volcaniclastics, tholeiites and andesites. The overlying Upper Ordovician is mainly composed of slightly metamorphosed clastics, volcanics with minor marble. These rocks belong to a series of Ordovician to Permian island arc, created by south-dipping subduction of the Kalamaili oceanic floor because there was an arc edifice located to the north and accretionary complex and ophiolitic fragments to the south (Ma et al., 1997; Xiao et al., 2004, 2008). The granitoids in Harlik area can be divided into late Ordovician to early Silurian (Cao et al., 2006; Ma et al., 2015), late Carboniferous (Sun et al., 2005; 2007), and Permian magmatism is characterized by the emplacement of abundant mafic-ultramafic intrusions (Zhou et al., 2004; Qin et al., 2011; Han et al., 2013; Song et al., 2013; Wang et al., 2014) and contemporaneous A-type granitoids (Yuan et al., 2010; Zhou et al., 2010; Chen et al., 2016; Shu et al., 2011; Mao et al., 2014).

3 Sample Descriptions and Analytical Methods

3.1 Sample descriptions

The Heiguniangshan pluton, located in the north of the Kalamaili fault, outcropped as an irregular batholith (110 km^2, Fig. 2), and the rock-types mainly are quartz diorite and monzogranite. Sample EJ16909-1 is fine-grained monzogranite collected from the eastern part of the pluton, which intruded into the early Carboniferous Nanmingshui Group. Notedly, the manzogranite developed into breccia-cataclastic rocks as a result of local structural events. It consists of plagioclase, K-feldspar and quartz. The accessory minerals include zircon, apatite, titanite and magnetite (Fig. 3).

The Akeshuoke pluton is located northeast of the Kalamaili fault and occupies an outcrop area of approximately 30 km^2 in East Junggar (Fig. 2). Sample EJ16910-1 is fine-grained monzogranite collected from the northern part of the pluton, which intruded into the early Carboniferous Batamayineishan Group, consisting of plagioclase (40%), K-feldspar (35–40%), quartz (20–25%) and biotite (3–5%). The accessory minerals include zircon, apatite, titanite and magnetite (Fig. 3).

The Guaishishan pluton, located in the southeast of the Kalamaili fault, has an area of approximately 28 km^2 in the Harlik area (Fig. 2). It is mainly composed of monzogranite with minor diabase dykes. The pluton was intrusive into Devonian volcanic-sedimentary rocks, the Dananhu Group. Sample EJ16910-3 is porphyritic

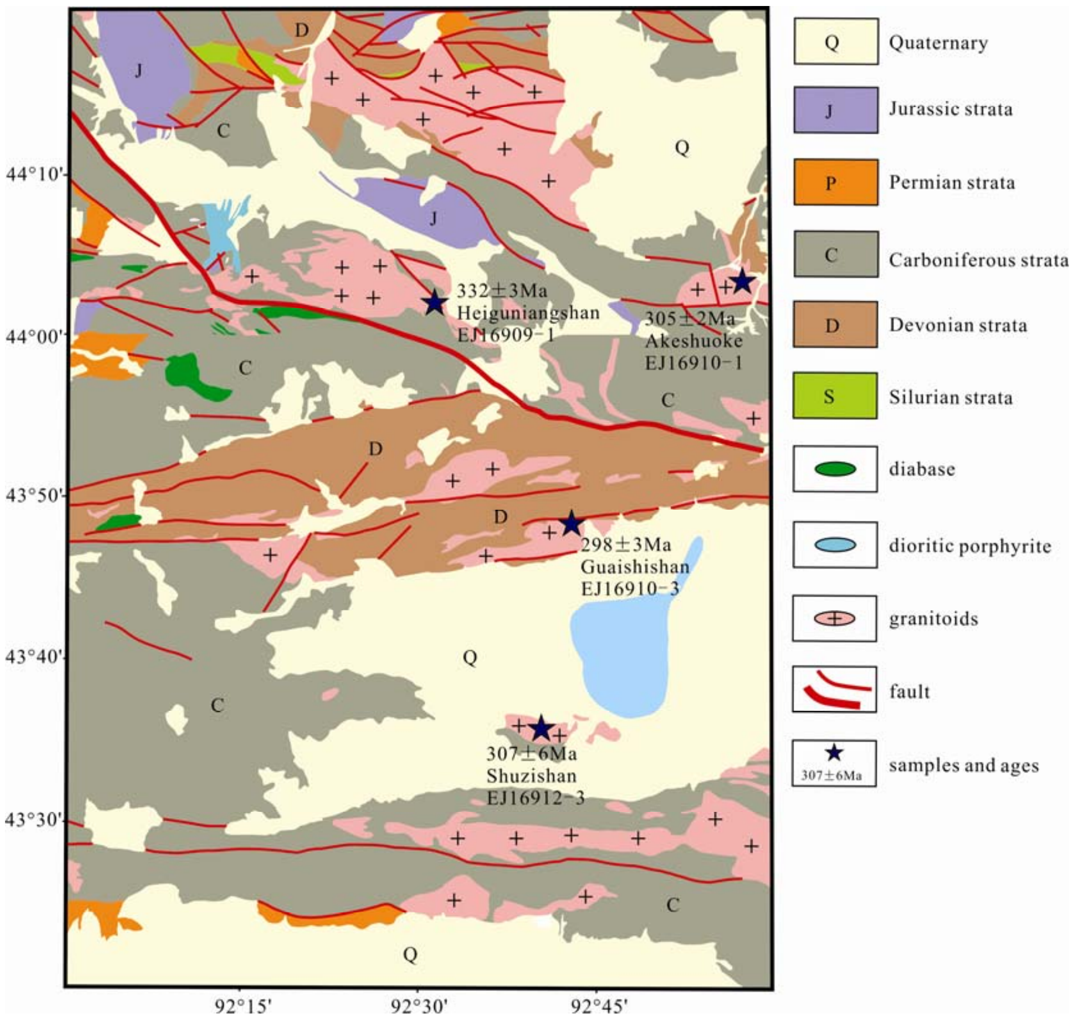

Fig. 2. Geological map of the studied area (after 1:200000 geological map of Barkol lake).

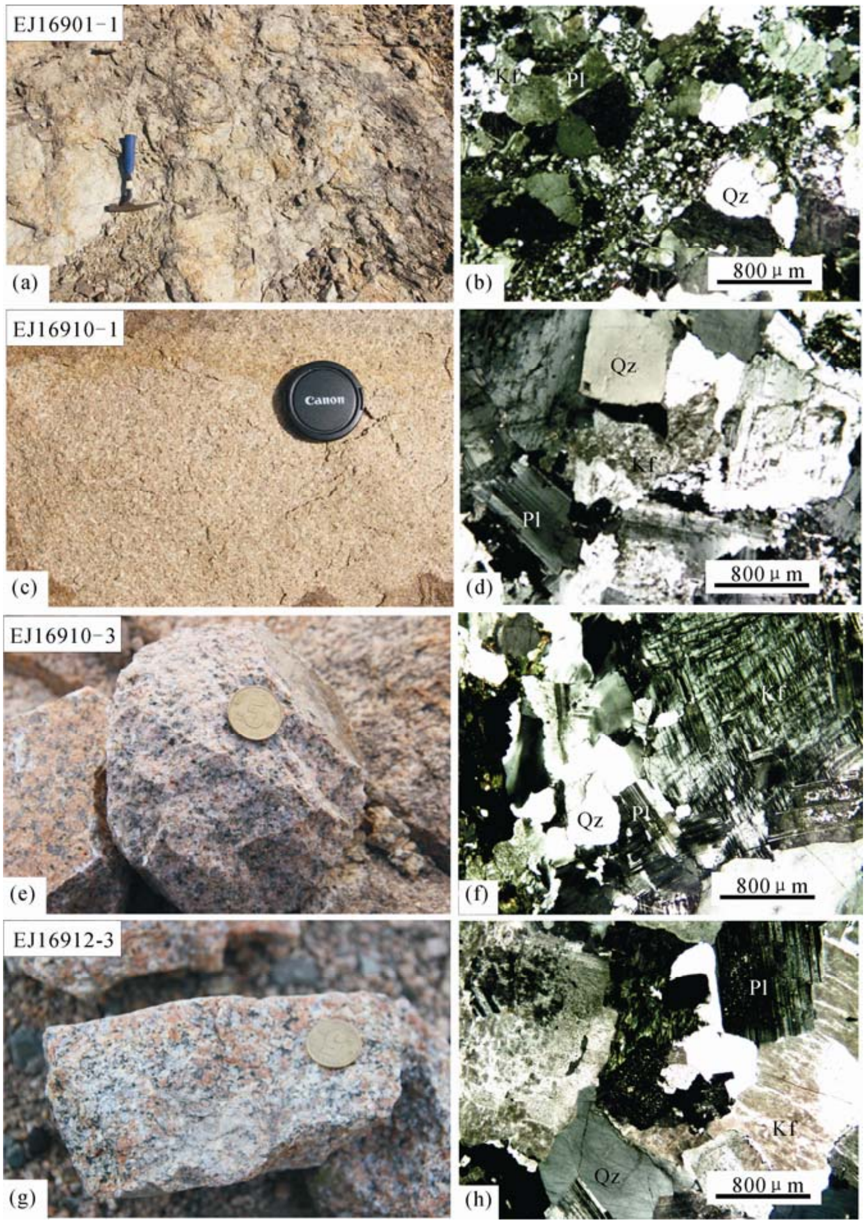

Fig. 3. Field photos (a, c, e, g) and photomicrographs (b, d, f, h) of granites from the Kalamaili fault zone.
Qz: Quartz, Kf: K-feldspar, Pl: Plagioclase. (a, b) monzogranite from Heiguniangshan pluton; (c, d) monzogranite from Akeshuoke pluton; (e, f) porphyritic monzogranite from Guaishishan pluton; (g, h) monzogranite from Shuzishan pluton

monzogranite collected from the northeastern part of the Guaishishan pluton. The phenocrysts are composed of plagioclase (5–10%) and quartz (5%), and the groundmass are composed of plagioclase (35–40%), K-feldspar (30–35%), quartz (20%) and biotite (5%). The accessory minerals are zircon, apatite and magnetite (Fig. 3).

The Shuzishan pluton is adjacent to the Balikun Lake in the southwest and occupies a small area of approximately 15 km^2, and intrude into Carboniferous volcanic-sedimentary rocks in the south of Harlik area (Fig. 2). The pluton is composed of gabbro (308±3 Ma, Lei et al., 2016a), monzogranite and syenogranite (302±2 Ma, Lei et al., 2016b). Sample EJ16912-3 is medium-fine grained monzogranite collected from the southern part of the Shuzishan pluton, consisting of plagioclase (40–45%), K-feldspar (30–35%), quartz (25%) and biotite (3–5%). The accessory minerals include zircon, apatite, titanite and others (Fig. 3).

3.2 Analytical methods

Cathodoluminescence (CL) imaging of polished zircons embedded in epoxy was conducted on a JEOL scanning electron microscope. LA-ICP-MS in-situ zircon analysis was carried out on an Agilent 7500A ICP-MS, equipped with a GeoLas 200M laser ablation system (MicroLas, Göttingen, Germany), at the State Key Laboratory of Continental Dynamics, Northwest University, Xi'an. The spot size was 30μm. Zircon 91500 and glass standard NIST SRM 610 were used as external standards for the age and concentration calculation, respectively, and ^{29}Si

(32.8% SiO_2) was chosen as the internal standard. Isotope ratios and elemental concentrations were calculated and plotted using the GLITTER 4.0 software (Macquarie University). For common Pb correction, the software of Andersen (2002) was employed, and the age calculations were performed with Isoplot 3.71 (Ludwig, 2008).

Major and trace elements for 20 samples were analysed at Acme Analytical Laboratories Ltd., Vancouver, Canada. Major element compositions and Sc, Ba, and Ni abundances were determined by inductively coupled plasma atomic emission spectroscopy (ICPAES). The remainder of the trace elements and rare earth elements (REE) were determined by ICP-MS. Loss on ignition (LOI) was determined by the weight difference after ignition at 1000°C. For major and trace element analysis, 0.20 g of the rock-powder was fused with 1.50 g of $LiBO_2$ and the pulps were dissolved in100 ml of 5% HNO_3. For ICP-MS analysis, 0.25 g of rock-powder was dissolved using four acid digestions. The detection limits varied between 0.01 and 0.1 wt% for the major oxides, 0.1 and 10 ppm for the trace elements, and 0.01 and 0.5 ppm for the REE. The analytical precision, as calculated from replicate analyses, was 0.5% for the major elements and varied from 2 to 20% for the trace elements.

Zircon Hf isotopic analyses were conducted using a Neptune MC-ICP-MS equipped with a New Wave UP193FX laser-ablation microprobe at the State Key Laboratory for Mineral Deposits Research, Nanjing University, China. Instrumental conditions and data acquisition methods are described in detail by Hou et al. (2007) and Wu et al. (2007). A stationary spot was used for the analyses, with a beam diameter of 35 μm. Helium was used as a carrier gas to transport the ablated sample from the laser ablation cell to the ICP-MS torch via a mixing chamber, where the helium was mixed with argon. Zircon 91500 was used as the reference standard and yielded a weighted mean $^{176}Hf/^{177}Hf$ ratio of 0.282308±12 during the analyses.

4 Results

4.1 U-Pb zircon results

Zircon grains from four samples range from 80 to 140 μm in size and have length to width ratios between 1:1 and 2:1, and they are mostly colorless, transparent and euhedral prismatic crystals. Most of zircon CL images exhibit magmatic oscillatory zoning (Fig. 4). The zircon U-Pb results are listed in Table 1.

Twenty-four zircon grains from monzogranite (sample EJ16909-1) of the Heiguniangshan pluton were analyzed and had low Th/U ratios (0.61–0.87). Ten zircon analyses yield $^{206}Pb/^{238}U$ ages from 330 to 334 Ma, with a weighted mean of 332±3 Ma (Fig. 5a), which is interpreted as the intrusion age of the pluton. Twelve discordant analyses are discarded because of analytical problems or incorrect common lead correction. In addition, two analyses show the $^{206}Pb/^{238}U$ ages of 397 Ma and 478 Ma, suggesting they are inherited zircons or xenocrysts.

Twenty-two zircon grains from monzogranite (sample EJ16910-1) of the Akeshuoke pluton were analyzed and had broad Th/U ratios (0.34–1.12). Twenty-one zircon analyses yield $^{206}Pb/^{238}U$ ages ranging from 297 to 309

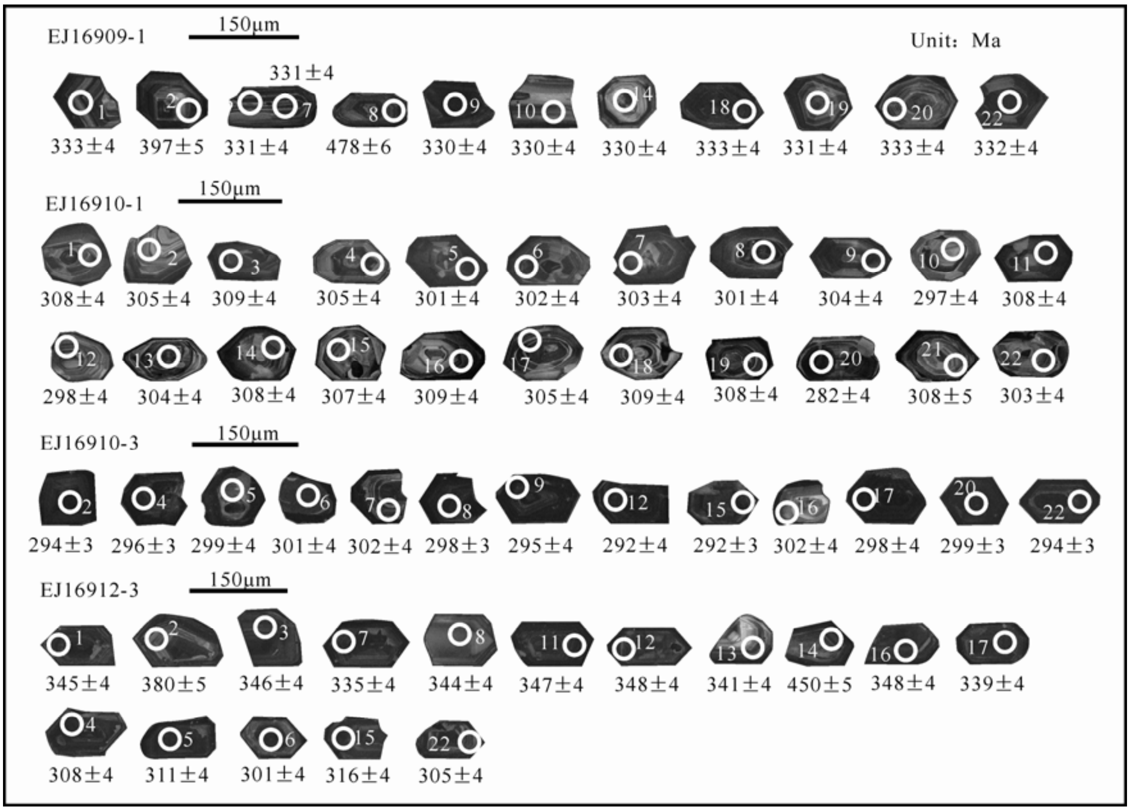

Fig. 4. Zircon CL images of granites from the Kalamaili fault zone. The locations of U-Pb spot analyses are shown as white circles.

Table 1 Zircon U-Pb age dating results

Spots	Contents (ppm)		Th/U	Ratios						Ages (Ma)					
	^{232}Th	^{238}U		^{207}Pb/^{206}Pb	1σ	^{207}Pb/^{235}U	1σ	^{206}Pb/^{238}U	1σ	^{207}Pb/^{206}Pb	1σ	^{207}Pb/^{235}U	1σ	^{206}Pb/^{238}U	1σ
Heiguniangshan															
EJ16909-1.1-01	386.24	476.61	0.81	0.05969	0.00179	0.43596	0.01062	0.05297	0.00067	593	63	367	8	333	4
EJ16909-1.1-02	121.79	181	0.67	0.05586	0.00187	0.4891	0.01391	0.0635	0.00083	446	73	404	9	397	5
EJ16909-1.1-03	611.23	592.64	1.03	0.06523	0.00172	0.47428	0.00949	0.05273	0.00064	782	55	394	7	331	4
EJ16909-1.1-04	1184.24	830.81	1.43	0.1211	0.00286	0.87923	0.01418	0.05265	0.00064	1973	41	641	8	331	4
EJ16909-1.1-05	279.05	444.03	0.63	0.07079	0.00209	0.51902	0.01228	0.05317	0.00068	951	59	425	8	334	4
EJ16909-1.1-06	278.28	399.78	0.70	0.05499	0.00153	0.40001	0.00868	0.05275	0.00064	412	60	342	6	331	4
EJ16909-1.1-07	285.63	440.79	0.65	0.05571	0.00148	0.40448	0.00821	0.05266	0.00064	440	58	345	6	331	4
EJ16909-1.1-08	418.39	523.08	0.80	0.05823	0.00152	0.61846	0.0121	0.07703	0.00093	538	56	489	8	478	6
EJ16909-1.1-09	262.8	317.1	0.83	0.05498	0.00209	0.39859	0.01336	0.05258	0.00073	411	82	341	10	330	4
EJ16909-1.1-10	155.85	223.15	0.70	0.0553	0.00192	0.40069	0.01193	0.05255	0.0007	424	75	342	9	330	4
EJ16909-1.1-11	1480.94	1331.93	1.11	0.17022	0.00384	1.1577	0.01687	0.04933	0.00059	2560	37	781	8	310	4
EJ16909-1.1-12	276.14	302.84	0.91	0.06799	0.00231	0.494	0.01426	0.0527	0.00071	868	69	408	10	331	4
EJ16909-1.1-13	213.24	264.46	0.81	0.06663	0.00204	0.48339	0.01208	0.05261	0.00068	826	63	400	8	331	4
EJ16909-1.1-14	125.92	196.09	0.64	0.05733	0.00236	0.41544	0.01533	0.05255	0.00076	504	89	353	11	330	5
EJ16909-1.1-15	860.66	630.34	1.37	0.11241	0.00261	0.81686	0.01277	0.0527	0.00063	1839	41	606	7	331	4
EJ16909-1.1-16	722.66	944.53	0.77	0.08692	0.00196	0.63441	0.00932	0.05293	0.00062	1359	43	499	6	333	4
EJ16909-1.1-17	777.66	692.05	1.12	0.07637	0.00199	0.55804	0.01091	0.05299	0.00065	1105	51	450	7	333	4
EJ16909-1.1-18	257.72	353.49	0.73	0.05585	0.00167	0.40834	0.00988	0.05303	0.00066	446	65	348	7	333	4
EJ16909-1.1-19	257.09	361.06	0.71	0.05388	0.00178	0.39111	0.01094	0.05264	0.00068	366	73	335	8	331	4
EJ16909-1.1-20	203.83	335.45	0.61	0.05334	0.00181	0.38947	0.01129	0.05296	0.00069	343	75	334	8	333	4
EJ16909-1.1-21	1043.86	579.4	1.80	0.13345	0.00386	0.96139	0.02176	0.05225	0.00071	2144	50	684	11	328	4
EJ16909-1.1-22	497.42	574.48	0.87	0.05507	0.00162	0.40176	0.00953	0.05291	0.00066	415	64	343	7	332	4
EJ16909-1.1-23	180.07	245.68	0.73	0.07424	0.00273	0.5385	0.01718	0.0526	0.00075	1048	72	437	11	331	5
EJ16909-1.1-24	279.55	361	0.77	0.07271	0.00283	0.52788	0.01804	0.05265	0.00077	1006	77	430	12	331	5
Akeshuoke															
EJ16910-1.1-01	189.86	298.97	0.64	0.05297	0.00161	0.35692	0.00885	0.04887	0.00061	328	67	310	7	308	4
EJ16910-1.1-02	102.48	225.01	0.46	0.05163	0.0017	0.34491	0.00958	0.04845	0.00062	269	74	301	7	305	4
EJ16910-1.1-03	454.35	426.66	1.06	0.05333	0.00173	0.36061	0.00984	0.04904	0.00063	343	72	313	7	309	4
EJ16910-1.1-04	227.17	302.9	0.75	0.06008	0.00206	0.40194	0.01179	0.04852	0.00064	607	73	343	9	305	4
EJ16910-1.1-05	260.38	454.35	0.57	0.05407	0.00154	0.35588	0.00805	0.04773	0.00059	374	63	309	6	301	4
EJ16910-1.1-06	322.1	425.44	0.76	0.05831	0.00216	0.38571	0.01244	0.04797	0.00066	541	80	331	9	302	4
EJ16910-1.1-07	220.35	265.43	0.83	0.05278	0.00167	0.34971	0.00921	0.04805	0.00061	319	70	305	7	303	4
EJ16910-1.1-08	347.47	766.59	0.45	0.05388	0.00151	0.35557	0.00785	0.04786	0.00059	366	62	309	6	301	4
EJ16910-1.1-09	301.65	420.18	0.72	0.05339	0.00208	0.35507	0.01228	0.04824	0.00067	345	86	309	9	304	4
EJ16910-1.1-10	205	279.21	0.73	0.05363	0.00173	0.34917	0.00945	0.04722	0.0006	356	71	304	7	297	4
EJ16910-1.1-11	228.2	381.73	0.60	0.0557	0.00152	0.37619	0.008	0.04898	0.0006	440	60	324	6	308	4
EJ16910-1.1-12	364.05	326.33	1.12	0.05425	0.0024	0.35403	0.01423	0.04733	0.0007	382	96	308	11	298	4
EJ16910-1.1-13	176.35	301.99	0.58	0.05354	0.0019	0.3561	0.01089	0.04824	0.00064	352	78	309	8	304	4
EJ16910-1.1-14	101.31	185.74	0.55	0.05356	0.00186	0.36093	0.01081	0.04887	0.00064	353	77	313	8	308	4
EJ16910-1.1-15	97.61	194.31	0.50	0.05444	0.00194	0.36632	0.01133	0.0488	0.00065	389	78	317	8	307	4
EJ16910-1.1-16	202.59	319.92	0.63	0.05346	0.00155	0.36129	0.0084	0.04902	0.00061	348	64	313	6	309	4
EJ16910-1.1-17	231.61	374.95	0.62	0.05734	0.00191	0.38332	0.01083	0.04848	0.00063	504	72	330	8	305	4
EJ16910-1.1-18	170.89	240.63	0.71	0.054	0.00176	0.36543	0.01	0.04908	0.00063	371	71	316	7	309	4
EJ16910-1.1-19	149.89	438.38	0.34	0.05189	0.0015	0.35053	0.00812	0.04899	0.0006	281	65	305	6	308	4
EJ16910-1.1-20	301.36	829.07	0.36	0.05379	0.00153	0.33206	0.00753	0.04477	0.00055	362	63	291	6	282	3
EJ16910-1.1-21	128.3	213.07	0.60	0.05565	0.00291	0.37521	0.01817	0.0489	0.0008	438	113	324	13	308	5
EJ16910-1.1-22	144.67	298.72	0.48	0.05398	0.00186	0.35871	0.01058	0.04819	0.00063	370	76	311	8	303	4
Guanshishan															
EJ16910-3.1-01	849.51	1288.74	0.66	0.06481	0.0017	0.41433	0.0082	0.04637	0.00056	768	54	352	6	292	3
EJ16910-3.1-02	723.13	816.93	0.89	0.05355	0.00132	0.34498	0.00619	0.04673	0.00055	352	55	301	5	294	3
EJ16910-3.1-03	1397.23	1672.1	0.84	0.09819	0.00222	0.64726	0.00961	0.04781	0.00056	1590	42	507	6	301	3
EJ16910-3.1-04	348.67	853.99	0.41	0.0532	0.0013	0.34402	0.00605	0.0469	0.00055	337	55	300	5	296	3
EJ16910-3.1-05	194.7	239.17	0.81	0.05243	0.00199	0.34366	0.01148	0.04754	0.00065	304	84	300	9	299	4
EJ16910-3.1-06	198.79	420.16	0.47	0.05195	0.0015	0.34277	0.0079	0.04785	0.00059	283	65	299	6	301	4
EJ16910-3.1-07	318.28	429.67	0.74	0.05425	0.00199	0.35861	0.01148	0.04794	0.00065	381	80	311	9	302	4
EJ16910-3.1-08	343.12	777.55	0.44	0.05356	0.00139	0.34984	0.00685	0.04737	0.00057	352	58	305	5	298	3
EJ16910-3.1-09	833.53	1227.83	0.68	0.05537	0.0015	0.35787	0.00753	0.04688	0.00057	427	59	311	6	295	4
EJ16910-3.1-10	798.19	1188.43	0.67	0.06969	0.00159	0.46555	0.0071	0.04845	0.00056	919	46	388	5	305	3
EJ16910-3.1-11	6888.59	4330.31	1.59	0.3936	0.00811	1.33564	0.01582	0.02461	0.00028	3885	31	861	7	157	2
EJ16910-3.1-12	501.15	826.75	0.61	0.05414	0.00156	0.34632	0.00798	0.04639	0.00057	377	63	302	6	292	4
EJ16910-3.1-13	39.88	83.5	0.48	0.05393	0.00298	0.36204	0.01869	0.04869	0.00081	368	119	314	14	307	5
EJ16910-3.1-14	334.18	607.65	0.55	0.05466	0.00155	0.33021	0.00744	0.04381	0.00054	398	62	290	6	276	3
EJ16910-3.1-15	773.67	1109.64	0.70	0.055	0.00146	0.35176	0.00712	0.04638	0.00056	412	58	306	5	292	3
EJ16910-3.1-16	111.83	165.31	0.68	0.05244	0.00211	0.34714	0.01248	0.04801	0.00067	305	89	303	9	302	4
EJ16910-3.1-17	452.14	1119.96	0.40	0.05858	0.0017	0.38224	0.00891	0.04733	0.00059	551	62	329	7	298	4
EJ16910-3.1-18	452.3	1038.66	0.44	0.11359	0.00256	0.72213	0.0107	0.0461	0.00054	1858	40	552	6	291	3
EJ16910-3.1-19	588.54	1219.96	0.48	0.05505	0.00157	0.33038	0.00753	0.04353	0.00054	414	62	290	6	275	3
EJ16910-3.1-20	577.75	1474.91	0.39	0.05255	0.00127	0.3442	0.00593	0.04751	0.00056	309	54	300	4	299	3
EJ16910-3.1-21	548.28	758.29	0.72	0.06275	0.00187	0.39532	0.00957	0.04569	0.00058	700	62	338	7	288	4
EJ16910-3.1-22	793.44	1856.97	0.43	0.05624	0.00139	0.36216	0.00653	0.0467	0.00055	461	54	314	5	294	3

Continued Table 1

Spots	Contents (ppm)		Th/U	Ratios						Ages (Ma)					
	^{232}Th	^{238}U		^{207}Pb/^{206}Pb	1σ	^{207}Pb/^{235}U	1σ	^{206}Pb/^{238}U	1σ	^{207}Pb/^{206}Pb	1σ	^{207}Pb/^{235}U	1σ	^{206}Pb/^{238}U	1σ
EJ16910-3.1-23	768.09	3471.65	0.22	0.08342	0.00178	0.53481	0.00698	0.0465	0.00053	1279	41	435	5	293	3
EJ16910-3.1-24	384.32	938.81	0.41	0.05922	0.00144	0.39976	0.00695	0.04896	0.00058	575	52	342	5	308	4
Shuzishan															
EJ16912-3.7-01	255.44	518.5	0.49	0.05378	0.00143	0.40754	0.00832	0.05495	0.00066	362	59	347	6	345	4
EJ16912-3.7-02	115.41	200.77	0.57	0.05497	0.00176	0.46057	0.01241	0.06076	0.00078	411	70	385	9	380	5
EJ16912-3.7-03	150.02	307.2	0.49	0.0547	0.00177	0.41631	0.01136	0.0552	0.00071	400	70	353	8	346	4
EJ16912-3.7-04	464.2	782.62	0.59	0.06013	0.00146	0.40629	0.00706	0.049	0.00058	608	52	346	5	308	4
EJ16912-3.7-05	367.72	683.09	0.54	0.05445	0.00147	0.3707	0.00771	0.04937	0.0006	390	59	320	6	311	4
EJ16912-3.7-06	472.29	808.17	0.58	0.05522	0.0017	0.36432	0.00927	0.04785	0.00061	421	67	315	7	301	4
EJ16912-3.7-07	336.32	607.11	0.55	0.05365	0.00138	0.39464	0.00763	0.05334	0.00064	357	57	338	6	335	4
EJ16912-3.7-08	167.52	167.22	1.00	0.05398	0.00197	0.40735	0.01296	0.05473	0.00073	370	80	347	9	344	4
EJ16912-3.7-09	447.04	606.87	0.74	0.08468	0.0021	0.64472	0.01156	0.05522	0.00067	1308	47	505	7	347	4
EJ16912-3.7-10	439.99	765.53	0.57	0.06068	0.00167	0.39865	0.00854	0.04764	0.00058	628	58	341	6	300	4
EJ16912-3.7-11	369.62	708.51	0.52	0.05491	0.00133	0.41846	0.00727	0.05527	0.00065	408	53	355	5	347	4
EJ16912-3.7-12	313.39	463.56	0.68	0.05775	0.0018	0.44201	0.01141	0.05551	0.00071	520	67	372	8	348	4
EJ16912-3.7-13	138.12	251.2	0.55	0.05822	0.00191	0.43641	0.01208	0.05436	0.00071	538	71	368	9	341	4
EJ16912-3.7-14	209.67	387	0.54	0.05794	0.00146	0.57804	0.01071	0.07236	0.00086	527	54	463	7	450	5
EJ16912-3.7-15	335.69	680.68	0.49	0.05327	0.00166	0.36869	0.00956	0.0502	0.00064	340	69	319	7	316	4
EJ16912-3.7-16	169.16	351.88	0.48	0.05461	0.0016	0.4179	0.00989	0.0555	0.00069	396	64	355	7	348	4
EJ16912-3.7-17	321.74	610.94	0.53	0.0546	0.00154	0.40628	0.00909	0.05396	0.00066	396	62	346	7	339	4
EJ16912-3.7-18	224.46	415.14	0.54	0.05665	0.0017	0.43705	0.01074	0.05595	0.00071	477	66	368	8	351	4
EJ16912-3.7-19	275.58	392.58	0.70	0.08821	0.00222	0.67467	0.01243	0.05547	0.00068	1387	47	524	8	348	4
EJ16912-3.7-20	293.28	594.43	0.49	0.0573	0.00201	0.41558	0.01261	0.0526	0.00071	503	76	353	9	331	4
EJ16912-3.7-21	1002.19	1267.7	0.79	0.14894	0.00327	1.10283	0.01542	0.0537	0.00063	2334	37	755	7	337	4
EJ16912-3.7-22	446.16	893.16	0.50	0.0561	0.00138	0.37479	0.00668	0.04845	0.00057	456	54	323	5	305	4
EJ16912-3.7-23	791.16	1313	0.60	0.1541	0.00326	1.18351	0.01522	0.0557	0.00064	2392	36	793	7	349	4
EJ16912-3.7-24	229.7	232.36	0.99	0.0577	0.00183	0.44255	0.01169	0.05563	0.00072	518	68	372	8	349	4

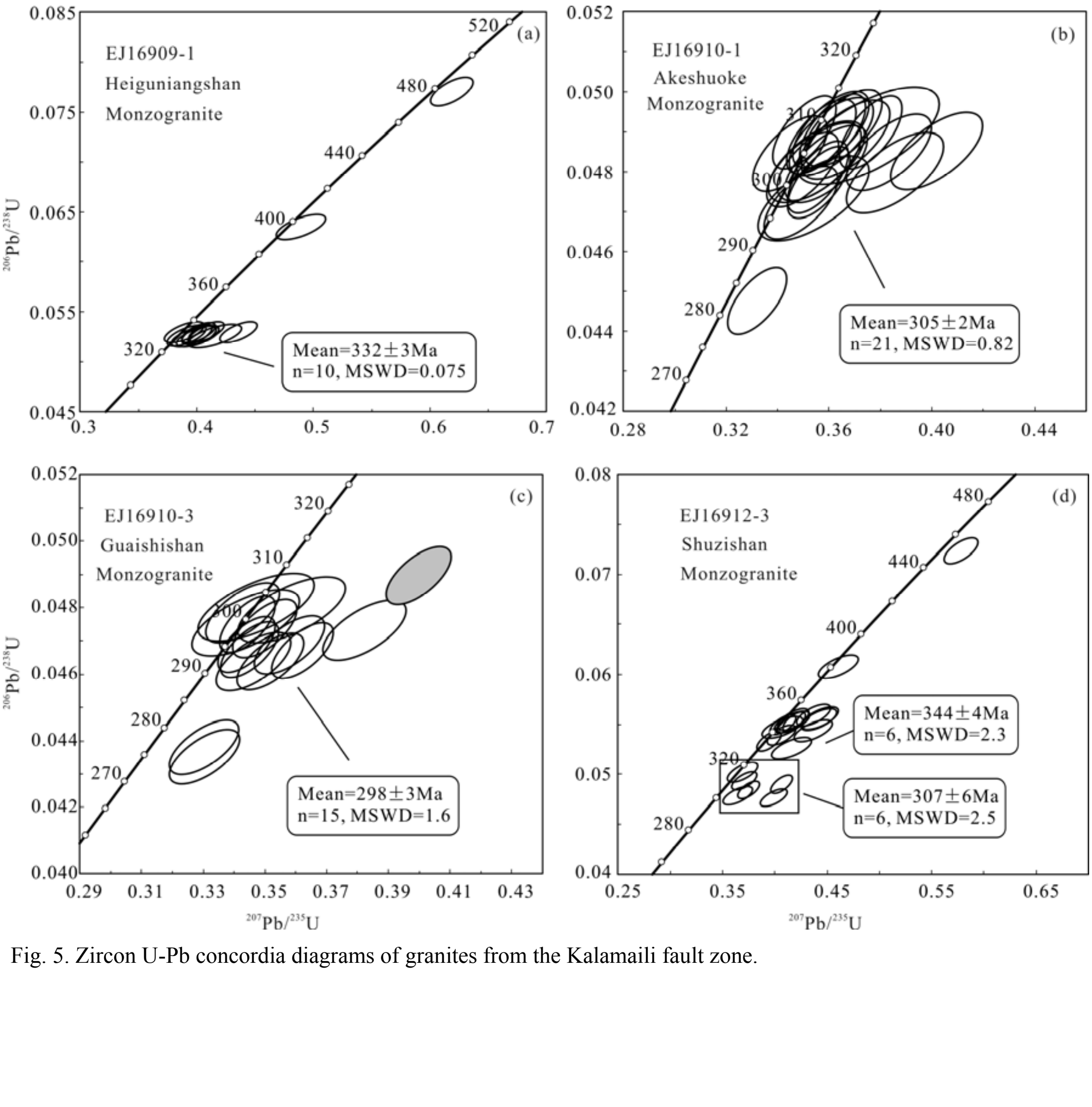

Fig. 5. Zircon U-Pb concordia diagrams of granites from the Kalamaili fault zone.

Ma, defining a weighted mean $^{206}Pb/^{238}U$ age of 305±2 Ma (Fig. 5b), interpreted as the formation age of the monzogranite. One other data point (spot 20) show much younger $^{206}Pb/^{238}U$ age of 282 Ma.

Twenty-four zircon grains from porphyritic monzogranite (sample EJ16910-3) of the Guaishishan pluton were analyzed and had low Th/U ratios (0.39–0.89). Fifteen spots yield $^{206}Pb/^{238}U$ ages ranging from 292 Ma to 308 Ma. These 15 analyses are concordant and yield a weighted mean $^{206}Pb/^{238}U$ age of 298±3 Ma (Fig. 5c), interpreted as the formation age of porphyritic monzogranite of the Guaishishan pluton. Seven discordant analyses are discarded because of analytical problems or incorrect common lead correction. In addition, two points (spots 14, 19) are younger with $^{206}Pb/^{238}U$ ages of 276 Ma and 275 Ma.

Twenty-four zircon grains from monzogranite (sample EJ16912-3) of the Shuzishan pluton were analyzed and had low Th/U ratios (0.48–1.00). Except for four spots (9, 19, 21, 23) with a high common lead contribution, the remaining eighteen analyses yield three age groups: (1) twelve spots on zircon core with $^{206}Pb/^{238}U$ ages from 331 Ma to 351 Ma (weighted mean $^{206}Pb/^{238}U$ age=344±4 Ma), which is similar to that of the Heiguniangshan granite which is near the Shuzishan pluton; (2) there are six spots on zircon core and rim with $^{206}Pb/^{238}U$ ages from 300 Ma to 308 Ma (weighted mean $^{206}Pb/^{238}U$ age =307±6 Ma) (Fig. 5d). The younger age of 307±6 Ma is considered as the emplacement age of the host granite, and the zircons dated at 344±4 Ma are either xenocrysts or antecrysts. In addition, two analyses show $^{206}Pb/^{238}U$ ages between 380 Ma and 450 Ma, suggesting they are inherited zircons or xenocrysts.

4.2 Whole rock elemental geochemistry

Whole-rock elemental geochemical data for the Carboniferous granitoids are listed in Table 2. The late Paleozoic granitoids have high contents in SiO_2 (72.91–77.64%, the Heiguniangshan pluton is the most evolved up to 77.64%) and K_2O (3.86–4.82%), moderate contents in Na_2O (3.49–4.47%) and low Fe_2O_3 (0.61–1.92%), MgO (0.08–0.46%) and CaO (0.34–1.11%) contents. They exhibit high-K calc-alkaline characteristics (Fig. 6a) and their A/CNK ratios range from 0.97 to 1.12, indicating they are weakly peraluminous (Fig. 6b, only one from Heiguniangshan pluton falls in the metaluminous field).

In the chondrite-normalized rare earth element diagram (Fig. 7a), the East Junggar granitoids have weakly fractionated REE patterns ($(La/Yb)_N$=4.61–8.17) with low total rare earth element contents (ΣREE=90.11–142.77 ppm), whereas the Harlik granitoids have weaklier fractionated REE patterns ($(La/Yb)_N$=3.18–6.18) with slightly higher total rare earth element contents (ΣREE=127.43–211.37 ppm). The East Junggar granitoids display large negative Eu anomalies (Eu/Eu^*=0.16–0.42), whereas the Harlik granitoids have similar Eu anomalies (Eu/Eu^*=0.17–0.37). In the primitive mantle-normalized spidergram (Fig. 7b), four plutons are all enriched in Rb, Th, U and light REEs, and depleted in high field strength elements (HFSE, such as Ta, Nb, Sr, P and Ti). All these features commonly observed in highly differentiated granitic rocks.

4.3 Zircon Hf isotopes

In-situ zircon Hf isotopic analyses from the samples analyzed for U-Pb ages are listed in Table 3 and presented in Fig. 10.

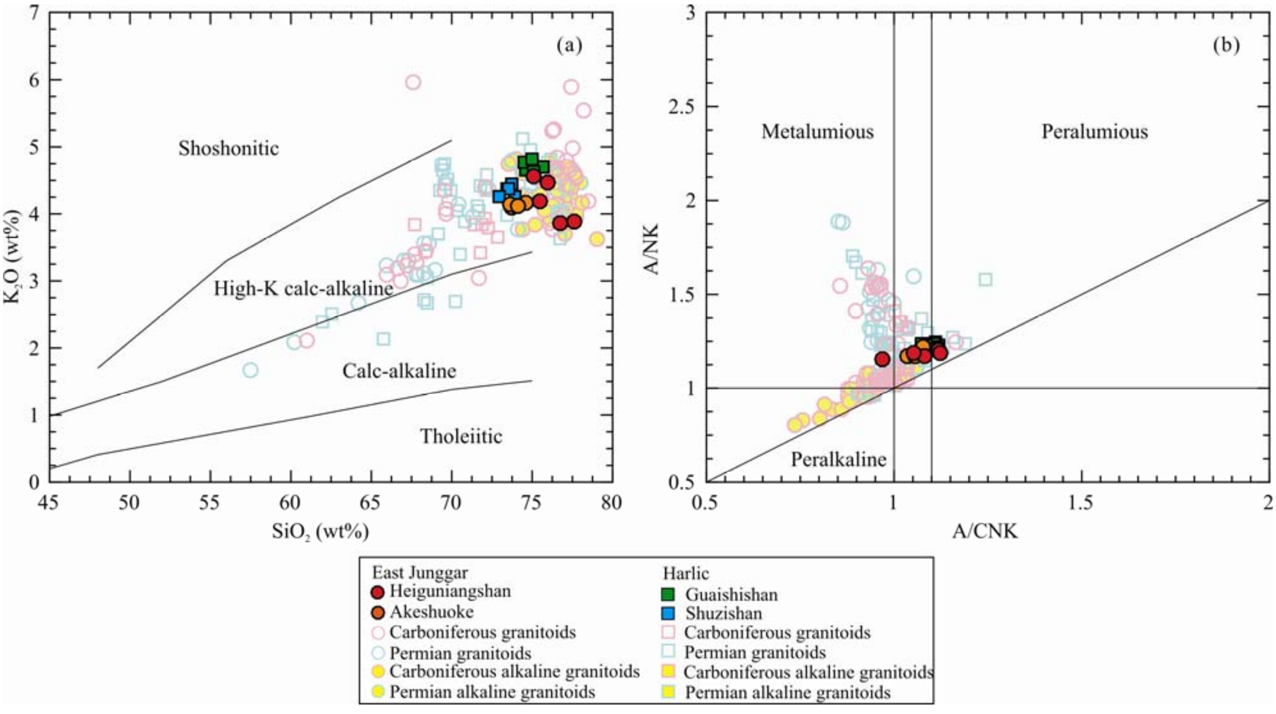

Fig. 6. Major element diagrams. (a) K_2O vs. SiO_2 diagram (after Peccerillo and Taylor, 1976), (b) A/NK vs. A/CNK diagram (after Maniar and Piccoli, 1989).

Data sources (East Junggar: Li et al., 2007; Su et al., 2008; Gan et al., 2010; Yang et al., 2009, 2010; Wang et al., 2010; Han et al., 2012; Liu et al., 2013. Harlik: Wang et al., 2009; Yuan et al., 2010; Chen et al., 2016; Song et al., 2018)

Table 2 Major elements (wt%) and trace elements (ppm) compositions of granites from the Kalamaili fault zone

No.	EJ16909-1.1	EJ16909-1.2	EJ16909-1.3	EJ16909-1.4	EJ16909-1.5	EJ16910-1.1	EJ16910-1.2	EJ16910-1.3	EJ16910-1.4	EJ16910-1.5
Age	332 Ma					305 Ma				
Pluton	Heiguniangshan					Akeshuoke				
Rock type	Monzogranite					Monzogranite				
SiO_2	75.12	76.01	75.52	76.73	77.64	73.71	74.03	74.58	73.63	74.15
Al_2O_3	13.62	13.14	13.14	12.03	12.72	14.26	14.17	13.76	14.36	13.82
$Fe_2O_3^T$	0.95	0.75	0.86	0.81	0.61	1.44	1.38	1.27	1.35	1.37
MgO	0.14	0.08	0.11	0.13	0.08	0.23	0.21	0.20	0.20	0.21
CaO	0.47	0.48	0.78	1.11	0.34	0.84	0.81	0.86	0.84	0.71
Na_2O	3.89	3.91	3.99	3.78	3.95	4.46	4.44	4.39	4.43	4.47
K_2O	4.55	4.46	4.18	3.86	3.89	4.10	4.11	4.16	4.15	4.11
TiO_2	0.12	0.11	0.11	0.10	0.09	0.19	0.18	0.16	0.18	0.18
P_2O_5	0.03	0.02	0.03	0.03	0.03	0.03	0.03	0.03	0.03	0.04
MnO	0.04	0.02	0.03	0.05	0.02	0.04	0.04	0.03	0.03	0.04
LOI	1.00	0.90	1.20	1.30	0.60	0.60	0.50	0.40	0.60	0.80
Total	99.94	99.94	99.94	99.95	99.95	99.92	99.93	99.93	99.91	99.92
A/CNK	1.12	1.08	1.05	0.97	1.12	1.07	1.07	1.04	1.08	1.06
$Mg^{\#}$	25.56	19.91	22.96	27.22	23.41	27.13	26.18	26.85	25.66	26.32
La	22.10	23.10	22.10	20.30	18.70	27.10	29.40	26.40	28.00	29.90
Ce	43.30	44.50	41.70	37.40	37.50	54.40	55.90	53.80	54.70	59.90
Pr	4.47	4.65	4.37	3.86	3.99	5.95	6.17	5.86	6.18	6.61
Nd	15.40	16.30	15.00	13.20	13.80	21.60	21.90	21.50	22.50	23.60
Sm	3.14	3.33	3.02	2.68	3.03	4.41	4.25	4.16	4.45	4.65
Eu	0.21	0.20	0.19	0.20	0.16	0.56	0.54	0.50	0.52	0.54
Gd	3.07	3.22	2.92	2.63	2.92	3.79	3.73	3.89	4.05	4.22
Tb	0.53	0.57	0.56	0.51	0.53	0.61	0.63	0.67	0.66	0.74
Dy	3.46	3.62	3.77	3.18	3.35	3.79	3.85	4.08	3.92	4.63
Ho	0.76	0.84	0.78	0.69	0.74	0.76	0.83	0.84	0.85	0.96
Er	2.53	2.75	2.60	2.23	2.48	2.49	2.40	2.55	2.62	2.92
Tm	0.37	0.41	0.39	0.38	0.39	0.36	0.38	0.41	0.37	0.46
Yb	2.80	2.87	2.83	2.46	2.91	2.42	2.58	2.67	2.78	3.19
Lu	0.41	0.44	0.43	0.39	0.42	0.37	0.40	0.40	0.40	0.45
Y	24.00	25.90	26.00	22.20	25.40	23.80	25.10	24.90	27.90	30.10
ΣREE	102.55	106.80	100.66	90.11	90.92	128.61	132.96	127.73	132.00	142.77
δEu	0.21	0.19	0.20	0.23	0.16	0.42	0.41	0.38	0.37	0.37
$(La/Yb)_N$	5.66	5.77	5.60	5.92	4.61	8.03	8.17	7.09	7.22	6.72
Ba	252	234	225	234	226	709	673	652	661	679
Co	0.80	0.40	0.40	0.50	0.40	1.10	0.80	0.80	0.60	0.90
Cs	3.00	3.10	2.90	2.40	2.00	2.90	2.80	2.90	3.30	3.10
Ga	12.00	10.00	10.80	9.10	9.70	15.60	14.40	14.20	15.40	15.10
Hf	6.30	6.10	5.90	5.70	5.50	8.30	8.10	8.10	10.30	8.50
Nb	8.00	7.50	8.70	6.40	8.50	7.00	7.10	5.10	7.70	7.80
Rb	145.90	138.10	135.50	118.80	133.60	90.80	91.30	88.70	97.50	104.60
Sr	60.40	63.10	58.70	62.60	47.00	87.30	79.30	75.70	77.70	80.70
Ta	1.10	0.90	1.30	0.80	1.20	0.70	0.70	0.50	0.90	0.80
Th	18.30	17.40	18.60	16.60	16.10	9.30	9.40	9.90	9.70	11.10
U	3.80	2.10	3.50	2.80	2.80	1.70	2.10	2.10	1.90	2.10
V	8.00	8.00	10.00	8.00	8.00	8.00	8.00	8.00	8.00	8.00
Zr	214.60	223.00	205.60	185.70	191.60	315.00	304.10	291.80	381.00	308.90
Zn	11.00	6.00	7.00	9.00	7.00	27.00	26.00	26.00	26.00	27.00
Ni	0.40	0.20	0.40	0.40	0.80	1.00	0.60	1.10	0.60	0.80
Cu	0.60	0.50	0.60	0.50	0.40	1.90	1.60	1.70	1.70	1.80
Pb	9.10	8.70	8.70	13.90	8.60	5.10	5.20	4.80	4.70	6.10
No.	EJ16910-3.1	EJ16910-3.2	EJ16910-3.3	EJ16910-3.4	EJ16910-3.5	EJ16912-3.10	EJ16912-3.11	EJ16912-3.7	EJ16912-3.8	EJ16912-3.9
Age	298 Ma					307 Ma				
Pluton	Guaishishan					Shuzishan				
Rock type	Porphyritic monzogranite					Monzogranite				
SiO_2	74.61	74.53	75.68	75.07	75	73.75	73.42	73.89	73.55	72.91
Al_2O_3	13.64	13.81	13.27	13.48	13.6	13.94	13.94	13.75	13.99	14.06
$Fe_2O_3^T$	1.4	1.38	1.21	1.41	1.41	1.66	1.89	1.88	1.9	1.92
MgO	0.16	0.16	0.15	0.17	0.19	0.41	0.4	0.46	0.39	0.4
CaO	0.92	0.73	0.63	0.78	0.56	0.62	0.79	0.76	0.62	0.89
Na_2O	3.66	3.66	3.49	3.64	3.64	3.97	4.01	3.89	4.19	4.19
K_2O	4.65	4.76	4.71	4.63	4.82	4.45	4.37	4.26	4.37	4.25
TiO_2	0.13	0.13	0.11	0.14	0.14	0.22	0.24	0.26	0.24	0.25
P_2O_5	0.03	0.03	0.02	0.03	0.03	0.04	0.05	0.05	0.05	0.05
MnO	0.04	0.03	0.03	0.03	0.03	0.04	0.04	0.05	0.04	0.04
LOI	0.7	0.7	0.6	0.5	0.5	0.7	0.7	0.6	0.5	0.9
Total	99.9	99.91	99.92	99.91	99.91	99.9	99.91	99.89	99.9	99.89
A/CNK	1.07	1.10	1.11	1.09	1.11	1.12	1.09	1.11	1.10	1.07
$Mg^{\#}$	21.03	21.27	22.41	21.93	23.90	36.53	33.03	36.32	32.36	32.68
La	34	22.6	24.1	28.6	28.3	21.7	35.3	29.1	42.1	34.2
Ce	71.2	47.4	51.6	60.2	57	61.4	74.2	66.5	87	72.4
Pr	8.16	5.41	5.66	6.71	6.32	5.98	8.45	7.56	9.86	8.41

Continued Table 2

No.	EJ16910-3.1	EJ16910-3.2	EJ16910-3.3	EJ16910-3.4	EJ16910-3.5	EJ16912-3.10	EJ16912-3.11	EJ16912-3.7	EJ16912-3.8	EJ16912-3.9
Age	298 Ma					307 Ma				
Pluton	Guaishishan					Shuzishan				
Rock type	Porphyritic monzogranite					Monzogranite				
Nd	30.6	20.1	21.4	24.7	23.7	24.3	32.5	30.6	35.8	33.4
Sm	6.99	5.43	4.85	5.54	5.07	5.83	6.93	6.42	7.32	7.12
Eu	0.39	0.35	0.34	0.39	0.37	0.71	0.74	0.74	0.84	0.76
Gd	7.18	5.91	5.16	5.67	4.91	5.82	6.62	6.97	7.23	7.2
Tb	1.31	1.05	0.99	1.06	0.88	1.05	1.11	1.2	1.19	1.26
Dy	8.22	6.62	6.19	7	5.44	6.32	7.02	7.51	7.44	8.08
Ho	1.77	1.44	1.37	1.51	1.25	1.37	1.5	1.64	1.52	1.67
Er	5.6	4.59	4.5	4.82	3.79	4.28	4.66	4.99	4.73	5.21
Tm	0.82	0.69	0.67	0.74	0.59	0.64	0.68	0.74	0.71	0.79
Yb	5.77	5.09	4.74	5.37	4.17	4.39	4.78	4.95	4.89	5.31
Lu	0.88	0.75	0.73	0.78	0.64	0.67	0.71	0.75	0.74	0.86
Y	52.5	42.3	40	44.8	37.1	40.3	41.9	47.5	42.7	47.6
ΣREE	182.89	127.43	132.3	153.09	142.43	144.46	185.2	169.67	211.37	186.67
δEu	0.17	0.19	0.21	0.21	0.23	0.37	0.33	0.34	0.35	0.32
$(La/Yb)_N$	4.23	3.18	3.65	3.82	4.87	3.55	5.30	4.22	6.18	4.62
Ba	225	238	243	250	267	517	497	482	523	523
Co	0.9	0.9	0.7	0.8	0.5	1.8	1.8	1.9	1.9	2
Cs	2.4	2.5	2	2	2.2	1.5	2	1.5	1.3	2
Ga	16.6	17.5	15.4	16.1	15.6	12.9	15	13.5	13.6	15.1
Hf	8.5	8.5	8.1	7.6	7.9	10.1	8.9	11.8	9.3	10
Nb	11.6	11.7	11.6	12	11.1	8.6	9.7	10.6	9.8	10.9
Rb	188.6	206.6	186.7	192.5	206.6	113.4	114	113.1	117.5	114.7
Sr	64.6	59.6	60.5	64.4	58.1	65.3	70.7	58.6	52.8	67.9
Ta	1.5	1.7	1.5	1.6	1.2	0.8	1	0.7	0.9	1
Th	30.7	27.2	26.1	28.1	25.9	15.2	16.2	16.1	16.6	19.3
U	4.9	2.3	2.2	1.9	3.5	2.3	2.3	2	2.4	1.8
V	10	9	11	10	8	14	17	16	22	19
Zr	289.5	260.1	255.6	246.7	253.9	362.6	308.5	431.6	341.1	360.1
Zn	29.00	34	23	32	36	44	31	43	40	33
Ni	0.50	0.5	0.5	0.6	0.6	2.1	2	2.1	2.2	2
Cu	0.6	0.5	0.3	0.2	0.3	3.9	5.5	3.1	2	4.6
Pb	11.2	9.4	7.2	14.2	9.5	11.8	9.7	8.7	11.7	9.3

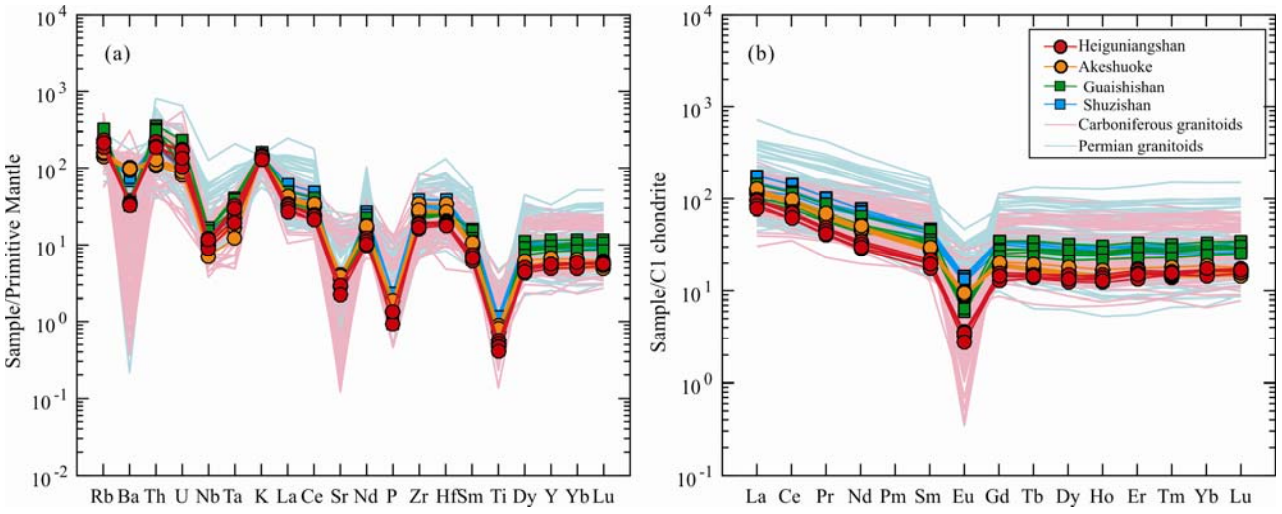

Fig. 7. (a) Primitive mantle-normalized trace element spider diagram and (b) chondrite-normalized rare earth element pattern. The values of chondrite and primitive mantle are from Sun and Mcdonough (1989). Data sources are listed in Fig. 6.

Eleven zircon grains from monzogranite (sample EJ16909-1) of the Heiguniangshan pluton were analyzed. Nine of them, with a weighted mean $^{206}Pb/^{238}U$ age of 332±3 Ma, have variable Hf isotopic compositions, with $^{176}Hf/^{177}Hf$ ratios of 0.282650–0.282806, $\varepsilon_{Hf}(t)$ values of +2.4 to +8.0 and two-stage Hf model ages (T_{DM2}) of 1.19–0.84 Ga. The inherited zircon with a $^{206}Pb/^{238}U$ age of ~397 Ma has a $^{176}Hf/^{177}Hf$ ratio of 0.282776, a positive $\varepsilon_{Hf}(t)$ value of +8.5 and young two-stage Hf model age (T_{DM2}) of 0.85 Ga. By comparison, the inherited zircon with an old $^{206}Pb/^{238}U$ age of ~478 Ma has a $^{176}Hf/^{177}Hf$ ratio of 0.282342, a negative $\varepsilon_{Hf}(t)$ value of −5.1 and old two-stage Hf model age (T_{DM2}) of 1.78 Ga.

Nineteen zircon grains from monzogranite (sample

Table 3 Zircon Hf isotopic compositions of granites from the Kalamaili fault zone

Spot.	Age (Ma)	^{176}Yb/^{177}Hf	^{176}Lu/^{177}Hf	^{176}Hf/^{177}Hf	2σ	ε_{Hf}(t)	T_{DM1} (Ma)	T_{DM2}(Ma)	$f_{Lu/Hf}$
16909-1.1-1	332	0.111513	0.003829	0.282663	0.000044	2.6	902	1177	-0.88
16909-1.1-2	333	0.086703	0.002800	0.282650	0.000034	2.4	896	1192	-0.92
16909-1.1-3	331	0.093478	0.003038	0.282713	0.000045	4.5	809	1056	-0.91
16909-1.1-4	333	0.085886	0.002695	0.282715	0.000019	4.7	797	1044	-0.92
16909-1.1-5	330	0.063697	0.002333	0.282719	0.000028	4.9	783	1031	-0.93
16909-1.1-6	330	0.054116	0.001612	0.282802	0.000015	8.0	648	833	-0.95
16909-1.1-7	330	0.073998	0.002592	0.282761	0.000039	6.3	727	941	-0.92
16909-1.1-8	478	0.045757	0.001371	0.282342	0.000024	-5.1	1299	1783	-0.96
16909-1.1-9	331	0.075740	0.002615	0.282806	0.000029	7.9	661	838	-0.92
16909-1.1-10	397	0.048982	0.001425	0.282776	0.000014	8.5	684	852	-0.96
16909-1.1-11	333	0.053494	0.001877	0.282739	0.000030	5.7	745	979	-0.94
16910-1.1-1	303	0.074960	0.002612	0.282866	0.000025	9.5	572	716	-0.92
16910-1.1-2	308	0.035586	0.001141	0.282898	0.000015	11.0	505	623	-0.97
16910-1.1-3	282	0.102423	0.003362	0.282923	0.000038	10.9	498	607	-0.90
16910-1.1-4	308	0.080193	0.002482	0.282902	0.000023	10.9	517	630	-0.93
16910-1.1-5	309	0.101610	0.003342	0.282832	0.000043	8.2	636	801	-0.90
16910-1.1-6	305	0.090568	0.002986	0.282858	0.000040	9.2	590	738	-0.91
16910-1.1-7	309	0.060980	0.001786	0.282935	0.000017	12.2	459	545	-0.95
16910-1.1-8	307	0.038351	0.001175	0.282931	0.000016	12.1	458	549	-0.96
16910-1.1-9	308	0.064483	0.001980	0.282898	0.000021	10.8	516	633	-0.94
16910-1.1-10	304	0.055424	0.001989	0.282822	0.000049	8.1	626	808	-0.94
16910-1.1-11	298	0.104220	0.003538	0.282758	0.000078	5.4	751	976	-0.89
16910-1.1-12	308	0.081846	0.002535	0.282875	0.000020	9.9	558	693	-0.92
16910-1.1-13	297	0.044445	0.001284	0.282905	0.000015	11.0	496	614	-0.96
16910-1.1-14	304	0.100346	0.003404	0.282878	0.000024	9.7	567	700	-0.90
16910-1.1-15	301	0.070417	0.002013	0.282949	0.000017	12.5	442	522	-0.94
16910-1.1-16	303	0.051433	0.001514	0.282921	0.000015	11.6	476	577	-0.95
16910-1.1-17	302	0.085190	0.002596	0.282821	0.000035	7.8	639	820	-0.92
16910-1.1-18	301	0.069979	0.002305	0.282849	0.000024	8.9	593	753	-0.93
16910-1.1-19	305	0.048071	0.001451	0.282897	0.000017	10.8	510	630	-0.96
16910-1.1-20	308	0.067264	0.001960	0.282907	0.000014	11.2	502	611	-0.94
16910-3.1-1	308	0.142031	0.004504	0.282902	0.000034	10.5	548	657	-0.86
16910-3.1-2	294	0.119135	0.003904	0.282843	0.000047	8.2	628	789	-0.88
16910-3.1-3	299	0.119560	0.003963	0.282840	0.000022	8.2	635	796	-0.88
16910-3.1-4	302	0.132208	0.003631	0.282784	0.000038	6.3	715	917	-0.89
16910-3.1-5	292	0.091333	0.002555	0.282877	0.000016	9.7	554	696	-0.92
16910-3.1-6	276	0.086285	0.003069	0.282870	0.000031	9.0	574	727	-0.91
16910-3.1-7	307	0.113386	0.002987	0.282930	0.000023	11.7	482	574	-0.91
16910-3.1-8	292	0.116333	0.003109	0.282965	0.000017	12.6	431	503	-0.91
16910-3.1-9	295	0.084756	0.002397	0.282894	0.000014	10.3	528	655	-0.93
16910-3.1-10	298	0.078808	0.002473	0.282874	0.000018	9.7	558	698	-0.93
16910-3.1-11	302	0.220284	0.005310	0.282934	0.000038	11.3	510	598	-0.84
16910-3.1-12	301	0.091780	0.002862	0.282893	0.000025	10.3	537	660	-0.91
16910-3.1-13	299	0.094702	0.002712	0.282852	0.000020	8.9	595	752	-0.92
16910-3.1-14	296	0.139701	0.004107	0.282755	0.000030	5.1	768	990	-0.88
16910-3.1-15	294	0.078095	0.002474	0.282841	0.000020	8.4	607	777	-0.93
16912-3.7-1	349	0.103308	0.003151	0.282875	0.000019	10.6	567	680	-0.91
16912-3.7-2	305	0.096322	0.002798	0.282873	0.000013	9.7	565	702	-0.92
16912-3.7-3	331	0.120586	0.003666	0.282886	0.000026	10.5	559	671	-0.89
16912-3.7-4	351	0.056317	0.001685	0.282848	0.000015	10.0	585	719	-0.95
16912-3.7-5	339	0.129880	0.003970	0.282840	0.000027	9.0	635	777	-0.88
16912-3.7-6	348	0.097015	0.003065	0.282832	0.000025	9.1	630	777	-0.91
16912-3.7-7	316	0.122092	0.003786	0.282878	0.000045	9.9	574	699	-0.89
16912-3.7-8	450	0.062396	0.002128	0.282688	0.000027	6.3	824	1033	-0.94
16912-3.7-9	348	0.104326	0.003275	0.282807	0.000034	8.1	673	838	-0.90
16912-3.7-10	341	0.065884	0.002159	0.282808	0.000037	8.3	650	822	-0.93
16912-3.7-11	347	0.062828	0.001872	0.282866	0.000013	10.5	560	682	-0.94
16912-3.7-12	300	0.078373	0.002290	0.282807	0.000014	7.4	653	847	-0.93
16912-3.7-13	344	0.100449	0.003028	0.282795	0.000030	7.7	686	863	-0.91
16912-3.7-14	335	0.109356	0.003076	0.282901	0.000015	11.2	527	627	-0.91
16912-3.7-15	301	0.122121	0.003859	0.282990	0.000035	13.6	402	452	-0.88
16912-3.7-16	311	0.122251	0.003913	0.282908	0.000048	10.8	530	635	-0.88
16912-3.7-17	308	0.081972	0.002439	0.282818	0.000016	7.9	641	822	-0.93
16912-3.7-18	346	0.072434	0.002330	0.282910	0.000043	12.0	502	588	-0.93
16912-3.7-19	380	0.066202	0.001978	0.282845	0.000016	10.4	593	714	-0.94
16912-3.7-20	345	0.081432	0.002317	0.282884	0.000015	11.0	541	650	-0.93

$\varepsilon_{Hf}(t) = \{[(^{176}Hf/^{177}Hf)_S-(^{176}Lu/^{177}Hf)_S \times (e^{\lambda t}-1)]/[(^{176}Hf/^{177}Hf)_{CHUR,0}-(^{176}Lu/^{177}Hf)_{CHUR} \times (e^{\lambda t}-1)]-1\} \times 10{,}000$,

$T_{DM} = 1/\lambda \times \ln\{1 + [(^{176}Hf/^{177}Hf)_S-(^{176}Hf/^{177}Hf)_{DM}]/[(^{176}Lu/177Hf)_S-(^{176}Lu/^{177}Hf)_{DM}]\}$,

$T_{DM2} = 1/\lambda\times\ln\{1 + [(^{176}Hf/^{177}Hf)_{S,t}-(^{176}Hf/^{177}Hf)_{DM,t}]/[(^{176}Lu/^{177}Hf)_C-(^{176}Lu/^{177}Hf)_{DM}]\} + t$, where, s = sample, $(^{176}Hf/^{177}Hf)_{CHUR,0} = 0.282772$, $(^{176}Lu/^{177}Hf)_{CHUR} = 0.0332$, $(^{176}Hf/^{177}Hf)_{DM} = 0.28325$, $(^{176}Lu/^{177}Hf)_{DM} = 0.0384$ (Blichert-Toft and Albarede, 1997; Griffin et al., 2000), t = crystallization age of zircon. $\lambda=1.865\times10^{-11}$ year^{-1} (Scherer et al., 2001). $(^{176}Lu/^{177}Hf)_C= 0.015$.

EJ16910-1) of the Akeshuoke pluton with a weighted mean $^{206}Pb/^{238}U$ age of 305±3 Ma have Hf isotopic compositions with $^{176}Hf/^{177}Hf$ ratios of 0.282821–0.282949, $\varepsilon_{Hf}(t)$ values of +7.8 to +12.5 and two-stage Hf model ages (T_{DM2}) of 0.82–0.52 Ga.

Twenty zircon grains from porphyritic monzogranite (sample EJ16910-3) of the Guaishishan pluton with a weighted mean $^{206}Pb/^{238}U$ age of 298±3 Ma have Hf isotopic compositions with $^{176}Hf/^{177}Hf$ ratios of 0.282755–0.282965, $\varepsilon_{Hf}(t)$ values of +5.1 to +12.6 and two-stage Hf model ages (T_{DM2}) of 0.99–0.50 Ga.

Twenty zircon grains from monzogranite (sample EJ16912-3) of the Shuzishan pluton were analyzed. Fourteen of them with a weighted mean $^{206}Pb/^{238}U$ age of 307 ± 6 Ma have Hf isotopic compositions with $^{176}Hf/^{177}Hf$ ratios of 0.282688–0.282910, $\varepsilon_{Hf}(t)$ values of +6.3 to +12.0 and two-stage Hf model ages (T_{DM2}) of 1.03–0.59 Ga. The remaining six zircons with a $^{206}Pb/^{238}U$ age of ~344 Ma has a high $^{176}Hf/^{177}Hf$ ratio of 0.282807–0.282990, positive $\varepsilon_{Hf}(t)$ value of +7.4 to +13.6 and young two-stage Hf model age (T_{DM2}) of 0.82–0.45 Ga.

5 Discussion

5.1 Genetic type

The Carboniferous granitoids in Kalamaili fault zone have high SiO_2 and K_2O contents, high differentiation index (DI=91.2–96.0) and show high-K calc-alkaline characteristics (Fig. 6a). In the spider diagram, the negative anomalies in Ba, P, Nb, Ta, Ti and Sr, pronounced positive anomalies in Rb, Th, K and La (Fig. 7a), suggesting that advanced fractional crystallization may have occurred during magma evolution and complex processes influenced by the compositions of the crustal rocks. Fractional crystallization was also confirmed by their REE patterns, which is characterized by strong Eu depletion. In the classification diagram, all samples plot into the field of highly fractionated calc-alkaline granite (Fig. 8a).

Most of these granites have A/CNK<1.1 and A/NK>1 (Fig. 6b). Their weak peraluminous characteristic simply they are not typical S-types. The negative correlation between P_2O_5 and SiO_2 appears to follow the I-type trend as same as the positive correlation between Th and Rb (Fig. 8b), which was considered as an effective means for distinction of I- from S-type granites by Chappell and White (1992). Thus, these four plutons are I-type or A-type, or more likely highly-evolved I-type granites.

These granites in NW China have some similarities to A-type in their field and petrographic characteristics. However, they do not contain mafic alkaline minerals such as arfvedsonite, riebeckite, etc. In the discrimination diagrams for A-type granite of Whalen et al. (1987), most samples straddle the fields of fractionated granites and A-type granites, suggesting their transitional character (Fig. 9). For example, in some discrimination diagrams of Nb, Ce vs. 10000´Ga/Al, the granites straddle the fields of A- and M-, I-, S-types with small variation in Ga/Al ratios (Fig. 9c–d). Furthermore, in FeO^T/MgO and $(K_2O+Na_2O)/CaO$ vs. (Zr +Nb+Ce+Y) diagrams, most samples of these granites fall in the field of highly fractionated I-type (Fig. 9a–b). We therefore conclude that the granites described in this study are highly fractionated I-type granites or transitional I-A type granites. Furthermore, in East Junggar and Harlik Mountain, the Carboniferous-Permian granitoids on both sides of Kalamaili fault zone are mostly high-K calc-alkaline, and alkaline rocks have appeared in this period (Fig. 6). The age of 332 Ma high-K calc-alkaline monzogranite identified in this paper provides critical evidence for the magma of the East Junggar orogen from calc-alkaline granite to 325 Ma alkaline granite.

5.2 Magma source

The newly obtained zircon U-Pb ages of 332±3 Ma, 305±2 Ma, 298±3 Ma and 307±6 Ma revealed two magma events of Early Carboniferous (332 Ma) and Late Carboniferous (307–298 Ma). They have different magma sources.

The late Carboniferous granitoids with chondritic positive zircon $\varepsilon_{Hf}(t)$ values (+5.1 to +13.6) and young Hf model ages (T_{DM2}= 0.99–0.45 Ga) (Fig. 10) indicate the

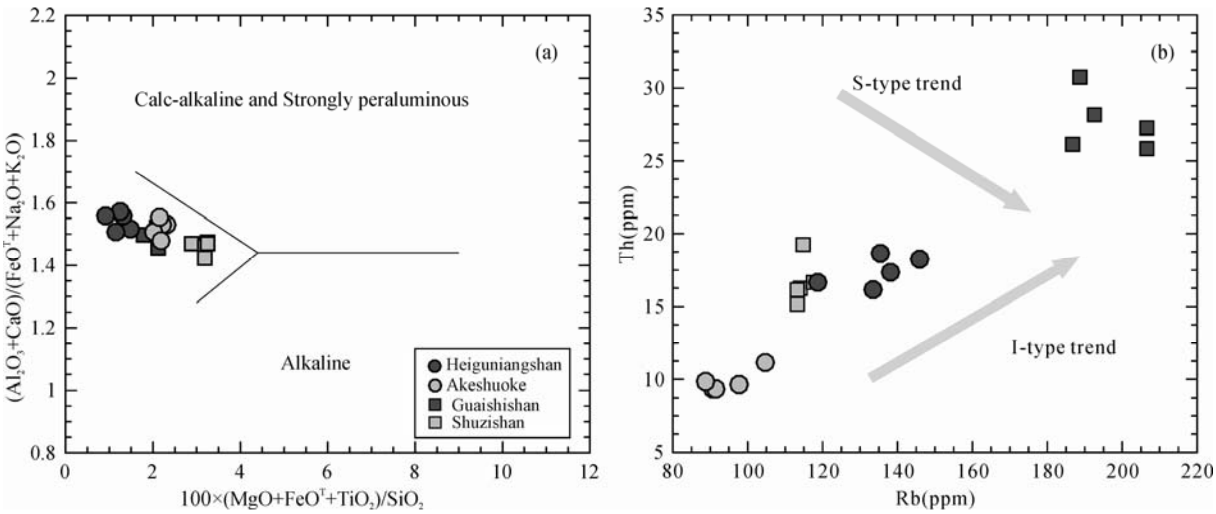

Fig. 8. (a) $100\times(MgO+FeO^T+TiO_2)/SiO_2$ versus $(Al_2O_3+CaO)/(FeO^T+Na_2O+K_2O)$ diagram (Sylvester (1989)); (b) Th vs. Rb variation diagrams showing that the granites follow the trend of I-type proposed by Chappell and White (1992).

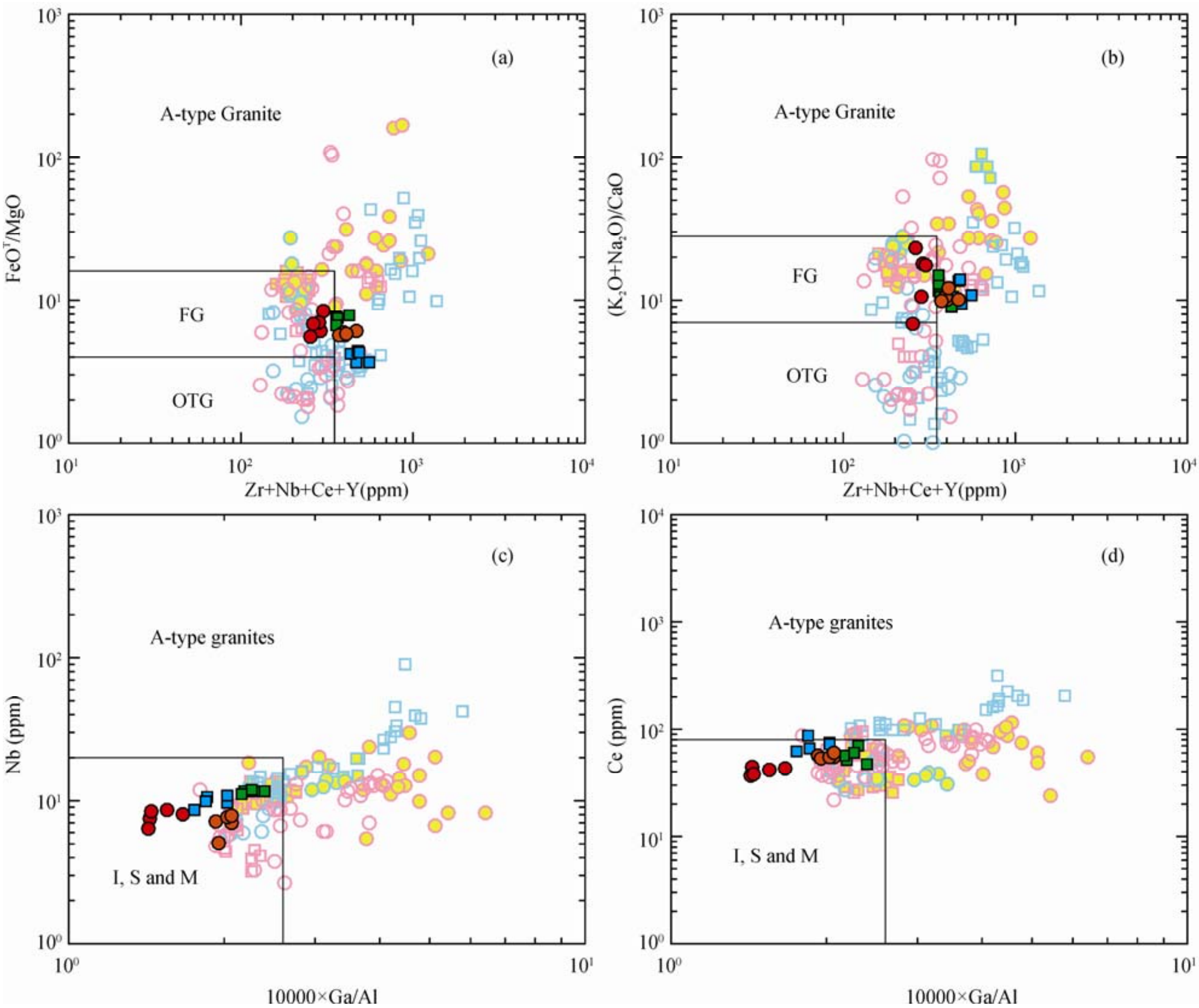

Fig. 9. (a) FeO^T/MgO, (b) (K_2O+Na_2O)/CaO vs. (Zr+Nb+Ce+Y) and (c) Nb, (d) Ce vs. 10000 Ga/Al classification diagrams (Whalen et al., 1987), indicating that the granites from the Kalamaili fault zone are transitional between the I-, S-, M- and A-types (a-d) or highly fractionated. FG: Fractionated felsic granites; OGT: unfractionated M-, I- and S-type granites. Symbols and data sources are the same as in Fig. 6.

involvement of juvenile components and minor old crust. The high $\varepsilon_{Hf}(t)$ values up to +13.6 suggest high proportion of juvenile materials. Combining with the occurrence of coeval basic/ultra basic magmas in the Sujishan pluton (308±3 Ma, Lei et al., 2016) and the Shiquanzi pluton (301±6 Ma, Yuan et al., 2010), indicating underplated mantle-derived basaltic magma provide material source and heat source. In addition, the $\varepsilon_{Hf}(t)$ values (+7.7 to +12.0) of the xenocrystic zircons (380–331 Ma) from Shuzishan pluton showing that late Devonian-early Carboniferous rocks were also involved in magma genesis.

However, the early Carboniferous granitoids in Heiguniangshan pluton with more chondritic positive zircon $\varepsilon_{Hf}(t)$ values (+2.4 to+ 8.0) and slightly younger Hf model ages (T_{DM2}=1.19–0.84 Ga) (Fig. 10) indicate the involvement of juvenile components and old crust. The $\varepsilon_{Hf}(t)$ values (−5.1and +8.5) of the Ordovician-Devonian xenocrystic zircons in these rocks show that Early-Middle

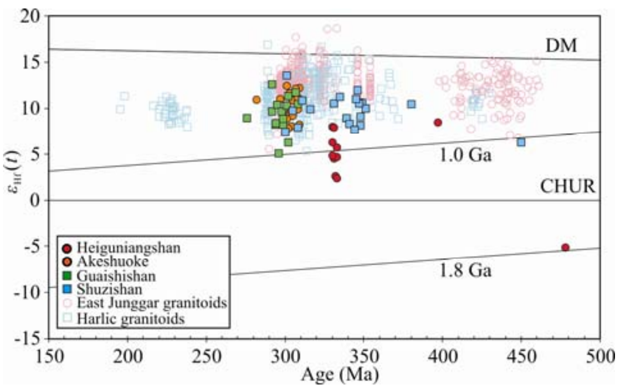

Fig. 10. $\varepsilon_{Hf}(t)$ vs. intrusive U-Pb age diagram.

Paleozoic rocks were involved in magma genesis, especially $\varepsilon_{Hf}(t)$ value of −5.1 suggesting more involvement of old continental composition. The presence of inherited xenocrystic zircons in Heiguniangshan monzogranite is also indicative of crustal assimilation or magma hybridization (e.g., Bonin, 2004). The Ordovician-Devonian ages of the inherited zircons correspond to igneous rocks of these ages in the Kalamaili area (Ma et al., 2015), suggesting that assimilated crustal materials were derived probably from the Ordovician-Devonian igneous rocks. Another possibility is that the xenocrysts probably originated as residual crystals during the melting of oceanic sediments because Ordovician-Devonian igneous rocks have positive $\varepsilon_{Nd}(t)$ values. Thus, it could have been acquired from partial melting of Paleozoic arc rocks that were deeply buried, together with trapped oceanic crust.

In summary, the Carboniferous granites were likely derived from a mixed source composed of juvenile mantle -derived materials and a small amount of old crustal source. But different sources between early Carboniferous and late Carboniferous granites are proposed. The source of the highly fractionated early Carboniferous I-type granite is relatively old, evidencing the involvement of ancient composition. We propose that the I-types were produced by melting of basic lower crust comprising mainly early Paleozoic oceanic crust and arc complex that were buried to a deep crust level by earlier tectonic processes (Chen et al., 2004; Xu et al., 2013). However, source for highly fractionated late Carboniferous I-type granite is characterized by voluminous new mantle-derived materials.

5.3 Petrogenesis

To account for the petrogenesis of these highly fractionated I-type granites, several processes can be envisaged: (a) differentiation of mantle-derived mafic magma (e.g. Han et al., 1997); (b) partial melting of a mixed source rock produced by intercalation of underplated mafic magma in lower crustal rocks (Wu et al., 2003; Li et al., 2007), and (c) mixing of mantle- and crustally derived magmas, which, in turn, underwent fractional crystallization (Chen et al., 2000; Qiu et al., 2008; Zhu et al., 2009; Tao et al., 2013). On the other hand, many petrogenetic models have been proposed for the origins of high-K calc-alkaline felsic I-type magmas, including: (1) crustal assimilation and fractional crystallization (AFC) of mantle-derived basaltic magma (Chen and Arakawa, 2005; Cribb and Barton, 1996; DePaolo,1981; Moghazi, 2003); (2) mixing of mantle derived magmas with crustal-derived materials (Clemens et al., 2009; Hildreth and Moorbath, 1988; Küster and Harms, 1998; Rottura et al.,1998; Yang et al., 2012). Thus, although the Early Carboniferous and Late Carboniferous have different material sources, mixing between mantle-derived magma (or juvenile crust) and crustal melt has also been proposed as a possible mechanism for generating highly fractional I-type granite.

As discussed above, the Carboniferous granites were likely derived from a mixed source composed of juvenile materials and a small amount of old crustal source. These young compositions are new underplating mantle-derived magma or juvenile lower crust. Based on Nd isotope data, Han et al. (1997) suggested that post-collisional granites were derived mainly by differentiation of underplated basic magmas. But Chen et al. (2004) proposed that the I-types were produced by melting of basic lower crust comprising mainly early Paleozoic oceanic crust and arc complex that were buried to a deep crust level by earlier tectonic processes. Our Hf isotopic data show that these granites did not come directly from the mantle but from a juvenile crust or a mantle-derived magma that had been contaminated by a pre-existing crustal component. Variably positive $\varepsilon_{Hf}(t)$ values suggest that these granites were probably derived from partial melting of juvenile crustal sources, and their distinct Hf isotopic compositions may indicate involvement of various amounts of recycled old crustal materials during their genesis.

Combined with the presence of voluminous coeval mafic intrusions (Yuan et al., 2010; Lei et al., 2016), upwelling of the hot asthenospheric mantle and/or decompression might have triggered the partial melting of the juvenile continental crust source underneath the East Junggar and Harlik to produce parental magmas that have formed early Carboniferous granitoids and the Kalamaili Fault may have acted as major channel for melt propagation. Then, advanced fractional crystallization has taken place during the formation of these granites. The low MgO, Fe_2O_3, Cr, Co, and Ni contents indicate that fractional crystallization of mafic minerals (e.g., clinopyroxene). Separation of Fe- and Mg-rich minerals, such as hornblende and biotite, may have occurred, as indicated by the negative correlation between total Fe_2O_3 and SiO_2 and between MgO and SiO_2. These granites show strong negative Eu anomalies, indicative of plagioclase separation.

Therefore, we suggest that the petrogenesis of the Carboniferous granitoids could be interpreted as a hybrid magma produced via both mantle- and crustal-derived melting and later experiencing strong fractional crystallization.

5.4 Tectonic implications

5.4.1 Post-collisional extension setting

Even if a lot of research on the granites on both sides of Kalamaili, the tectonic setting of the Carboniferous has controversial issues including：(1) post-collision environment (e.g. Chen et al., 2011; Tong et al., 2012, 2014), (2) the subduction environment (e.g., Xu et al., 2013; Zhang et al., 2018). The highly fractionated I-type granites are generally related to (1) anorogenic magmatism triggered by the breakup and foundering of a subducted flat slab beneath continental crust (Li et al., 2007), (2) post-orogenic magmatism (Wu et al., 2003), (3) subducted oceanic floor (Zhu et al., 2009), (4) the underplating of basaltic magmas, triggered by lithospheric delamination during the beginning of the post-orogenic episode (Chen et al., 2000). Furthermore, High-K calc-alkaline batholiths typically occur in post-collisional settings (Barbarin, 1999).

In the Nb vs. Y and Rb vs. (Y+Nb) diagrams (Fig. 11), the four studied highly fractionated I-type granites of Kalamaili area fall in the volcanic-arc field of Pearce et al. (1984). According to the criteria of Sylvester (1989), however, these rocks belong to post-collisional alkaline granites. Coeval felsic and mafic (~300 Ma, Yuan et al.,

2010) magmas are present in the area, indicating a typical bimodal igneous series in an extensional setting. In Fig. 11, all most samples fall into the VAG field, however, in this post-collisional period, subduction has already ceased, hence the arc geochemical signature of the granitoids is not related to subduction (Chen et al., 2004; Song et al., 2018). Instead, it could have been acquired from partial melting of Paleozoic arc rocks that were deeply buried, together with trapped oceanic crust. It should be as the post-collision progress, the mantle-derived material increases.

The late Paleozoic granitoids from the Kalamaili fault zone occur mainly in the post-collisional zone (Fig. 11). The types of these granitoids are I-, A-type and high fractionated granites (transitional I-A type), indicating a complicated background (Fig. 9). The existence of post-collisional early Permian igneous rocks in the Beishan, close to the studied area, has been used to support a change in geodynamic regime from compression to extension (Li et al., 2013b). The post-subduction arc-arc/continent collision may lead to crustal thickening and delamination of the subcontinental lithospheric mantle resulting in the upwelling of hot asthenospheric material, thus promoting melting and leading to underplating of new mafic magmas (Schott and Schmeling, 1998; Bonin, 2004; Lustrino, 2005; Richards, 2009).

From the perspective of magma source, combined with the regional geologic background, the Early Carboniferous should be the start of post-collision, while the Late Carboniferous was in the transition or post-collision period.

5.4.2 The closure time of Kalamaili Ocean

Large volumes of late Carboniferous to early Permian magmatic rocks in this region were probably emplaced in a post-collisional setting (e.g., Yuan et al., 2010). The Kalamaili oceanic crust should be subducted to the north beneath the East Junggar arc. The oceanic basin was finally consumed in the early Carboniferous, leading to the arc-continent collision of the Harlik-Dananhu arc onto the East Junggar arc (Han et al., 2018). Recent radiometric dating results suggests that the ophiolites along the Kalamaili suture zone formed in the period between ~417 and ~330 Ma (e.g., Wang et al., 2009). Taking all above evidence into account, we regard ~340 Ma as the closure time of the Kalamaili Ocean (Han et al., 2018). Our crystallization age of Heiguniangshan is 332±3 Ma, strongly supporting that the Kalamaili Ocean has been

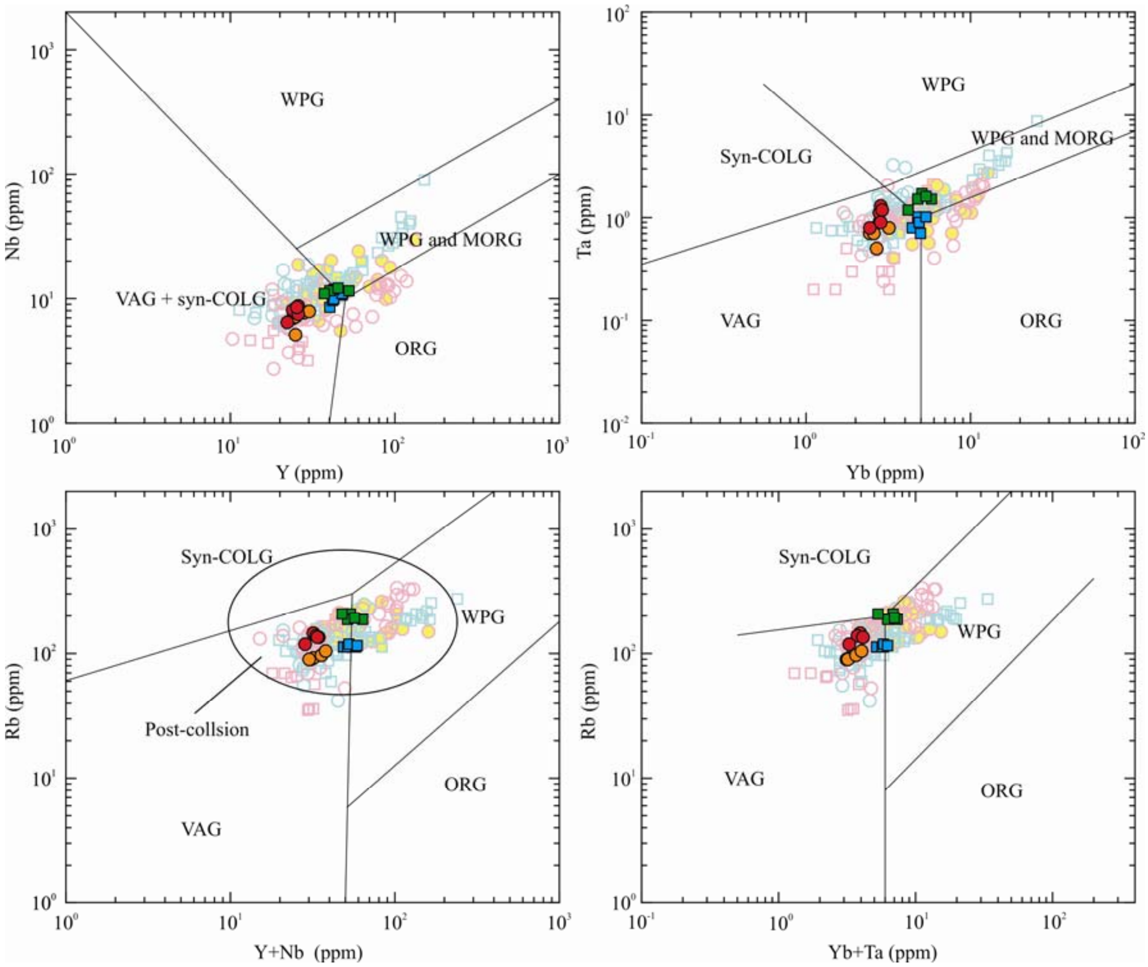

Fig. 11. Discrimination diagrams of tectonic setting of granitoids from the Kalamaili fault zone (after Pearce et al., 1984).

Symbols and data sources are the same as in Fig. 6. ORG — orogenic granites; syn-COLG — syn-collisional granites; VAG — volcanic arc granites; WPG — within plate granites closed in early Carboniferous.

5.5 Crustal growth

The CAOB is well-known for significant continental growth during the Phanerozoic (e.g., Jahn et al., 2000a, b, 2004; Song et al., 2019). As stated above, the production of post-collisional magmatic rocks by partial melting of the crust requires heat from the underplating of mantle-derived magmas. The resultant magmas produced a high temperature zone at the base of the crust, partial melting of the crustal rocks to generate highly fractionated I-type granite, and contributed to the source of the granitoids. Therefore, the vertical continental growth in the CAOB during the Carboniferous is also probably significant.

Most samples from East Junggar and Harlik show Hf model ages (T_{DM2}) younger than 1.0 Ga (Fig. 10), clearly indicating a juvenile nature of the crust in this area. Consequently, we believe that basaltic underplating is an important mechanism the subduction zone processes in the growth of the continental crust. The CAOB is the largest Phanerozoic accretion orogenic belt, and East Junggar and Harlik Mountain are the most prominent young crustal growth area.

6 Conclusions

(1) Early Carboniferous (332 Ma) and late Carboniferous (307–298 Ma) granitic magmatism have been recognized in Kalamaili fault zone. They are mainly metaluminous highly fractionated I-type and belong to the high-K calc-alkaline.

(2) Whole-rock geochemical and zircon isotopic tracing suggest that these granitoids were derived from heterogeneous source. These hybrid magma source to higher crustal levels and underwent fractional crystallization (AFC), as well as limited additional assimilation of old crustal materials. Our results show that the post-collision begun at 332 Ma and lasts until 298 Ma.

(3) They were formed in a post-collisional setting probably were linked to asthenospheric upwelling in response to a transition in the geodynamic setting from an arc-related setting to a post-collisional extensional setting in the southwestern CAOB.

Acknowledgements

This research was supported financially by the NSFC projects (U1403291, 41830216, and 41802074) and projects of the China Geological Survey (Nos. DD20160024, DD20160123, and DD20160345). This paper contributes to IGCP 662.

Manuscript received May 15, 2019
accepted Aug. 14, 2019
associate EIC XIAO Wenjiao
edited by FEI Hongcai

References

Barbarin, B., 1999. A review of the relationships between granitoid types, their origins and their geodynamic environments. Lithos, 46(3): 605–626.

Blichert-Toft, J., and Albarede, F., 1997. The Lu-Hf isotope geochemistry of chondritesand the evolution of the mantle-crust system. Earth and Planetary Science Letters, 148: 243–258.

Bonin, B., 2004. Do coeval mafic and felsic magmas in post-collisional to within-plate regimes necessarily imply two contrasting, mantle and crustal, sources? A review. Lithos, 78: 1–24.

Cao, F.G., Tu, Q.J., Zhang, X.M., Ren, Y., Li, S.L., and Dong, F.R., 2006. Preliminary determination of the Early Paleozoic magmatic arc in the Karlic Mountains, East Tianshan, Xinjiang, China—Evidence from zircon SHRIMP U-Pb dating of granite bodies in the Tashuihe area. Geological Bulletin of China, 25(8): 923–927(in Chinese with English abstract).

Cawood, P.A., Kröner, A., Collins, W.J., Kusky, T.M., Mooney, W.D., and Windley, B.F., 2009. Earth accretionary orogens through Earth history. In: Cawood, P.A., Kröner, A. (eds.), Earth Accretionary Systems in Space and Time. Geological Society of London, Special Publications, 318: 1–36.

Chappell, B.W., and White, A.J.R., 1992. I- and S-type granites in the Lachlan Fold Belt. Transactions of the Royal Society of Edinburgh: Earth Sciences, 83(1-2): 1–26.

Chen, B., and Jahn, B.M., 2004. Genesis of post–collisional granitoids and basement nature of the Junggar Terrane, NW China: Nd–Sr isotope and trace element evidence. Journal of Asian Earth Sciences, 23(5): 691–703.

Chen, B., and Arakawa, Y., 2005. Elemental and Nd-Sr isotopic geochemistry of granitoids from the West Junggar foldbelt (NW China), with implications for Phanerozoic continental growth. Geochimica et Cosmochimica Acta, 69: 1307–1320.

Chen, C.H., Lin, W., Lu, H.Y., Lee, C.Y., Tien, J.L., and Lai, Y.H., 2000. Cretaceous fractionated I-type granitoids and metaluminous A-type granites in SE China: the Late Yanshanian post-orogenic magmatism. Earth and Environmental Science Transactions of the Royal Society of Edinburgh, 91(1-2): 195–205.

Chen, X.J., Shu, L.S., and Santosh, M., 2011. Late Paleozoic post-collisional magmatism in the Eastern Tianshan Belt, Northwest China: new insights from geochemistry, geochronology and petrology of bimodal volcanic rocks. Lithos, 127: 581–598.

Chen X.J, Zhang KH, Zhang GL, and Zhou J. 2016. Characteristics, petrogenesis and tectonic implications of the Permian Omoertage alkaline granites in Harlik area, Xinjiang. Acta Petrologica ET Mineralogica, 35(6): 929–946 (in Chinese with English abstract).

Clemens, J.D., Darbyshire, D.P.F., and Flinders, J., 2009. Sources of post-orogenic calcalkaline magmas: the Arrochar and Garabal Hill–Glen Fyne complexes, Scotland. Lithos, 112: 524–542.

Cribb, J.W., and Barton, M., 1996. Geochemical effects of decoupled fractional crystallization and crustal assimilation. Lithos, 37: 293–307.

DePaolo, D.J., 1981. Trace element and isotopic effects of combined wallrock assimilation and fractional crystallization. Earth and Planetary Science Letters, 53: 189–202.

Gan, L., Tang, H.F., and Han, Y.J., 2010. Geochronology and geochemical characteristics of the Yemaquan granitic pluton in East Junggar, Xinjiang. Acta Petrologica Sinica, 26 (8): 2374–2388 (in Chinese with English abstract).

Griffin, W.L., Pearson, N.J., Belousova, E., Jackson, S.E., van Achterbergh E., O'Reilly, S.Y., and Shee, S.R., 2000. The Hf isotope composition of cratonic mantle: LAM-MC-ICPMS analysis of zircon megacrysts in kimberlites. Geochim Cosmochim Acta, 64: 133–147.

Gu, L., Hu, S., Chu, Q., Yu, C., and Xiao, X., 1999. Pre-collision granites and post-collision intrusiveassemblage of the Kelameili-Harlik orogenic belt: Acta Geologica Sinica (English Edition), 73:316–329.

Han, B.F., Wang, S.G., Jahn, B.M., Hong, D.W, Kagami H, and Sun, Y.L., 1997. Depleted mantle magma source for the Ulungur River A–type granites from north Xinjiang China: Geoch emistry and Nd–Sr isotopic evidence, and implication for Phanerozoic crustal growth. Chemical Geology, 138(3–4): 135–159.

Han, B.F., Ji, J.Q., Song, B., Chen, L.H., and Zhang L., 2006. Late Paleozoic vertical growth of continental crust around the Junggar Basin, Xinjiang, China (Part Ⅰ)：Timing of post–collisonal plutonism. Acta Petrologica Sinica, 22(5): 1077–1086 (in Chinese with English abstract).
Han, B.F., Guo, Z.J., and He, G.Q., 2010. Timing of major suture zones in North Xinjiang, China: constraints from stitching plutons. Acta Petrologica Sinica, 26: 2233–2246 (in Chinese with English abstract).
Han, C.M., Xiao, W.J., Zhao, G.C., Su, B.X., Ao, S.J., Zhang, J.E., and Wan, B., 2013. Age and tectonic setting of magmatic sulfide Cu-Ni mineralization in the Eastern Tianshan Orogenic Belt, Xinjiang, Central Asia. Journal of GEOsciences, 58: 233–250.
Han, Y.G., and Zhao, G.C., 2018. Final amalgamation of the Tianshan and Junggar orogenic collage in the southwestern Central Asian Orogenic Belt: Constraints on the closure of the Paleo-Asian Ocean. Earth-Science Reviews, 186: 129-152.
Hildreth, W., and Moorbath, S., 1988. Crustal contributions to arc magmatism in the Andes of Central Chile. Contributions to Mineralogy and Petrology, 98: 455–489.
Han, Y.J., Tang, H.F., and Gan, L., 2012. Zircon U-Pb Ages and Geochemical Characteristics of the Laoyaquan A-type Granites in East Junggar, North Xinjiang, China. Acta Mineralogica Sinica, 32(2): 193–199 (in Chinese with English abstract).
Hou, K.J, Li, Y.H., Zou, T.R., Qu, X.M., Shi, Y.R., and Xie, G.Q., 2007. Laser ablation MC–ICP–MS technique for Hf isotope microanalysis of zircon and its geological applications. Acta Petrologica Sinica, 23(10): 2595–2604 (in Chinese with English abstract).
Huang, G., Niu, G.Z., Wang, X.L., Guo, J., and Yu, F., 2012. Formation and emplacement age of Karamaili ophiolite: LA-ICP-MS zircon U-Pb age evidence from the diabase and tuff in eastern Junggar, Xinjiang. Geological Bulletin of China, 31: 1267–1278 (in Chinese with English abstract).
Huang, W., 2014. Geochoronology, geochemistry and origin of Carboniferous-Permian alkali granites in eastern Tianshan, Hami, NW China (master's thesis). Beijing: China University of Geosciences, 1–79 (in Chinese with English abstract).
Jahn, B.M., Wu, F.Y., and Chen, B., 2000a. Granitoids of the Central Asian Orogenic Belt and continental growth in the Phanerozoic. Transactions of the Royal Society of Edinburgh: Earth Sciences, 91(1–2): 181–193.
Jahn, B.M., Wu, F.Y., and Chen, B., 2000b. Massive granitoid generation in Central Asia: Nd isotope evidence and implication for continental growth in the Phanerozoic. Episodes, 23(2): 82–92.
Jahn, B.M., 2004. The Central Asian Orogenic Belt and growth of the continental crust in the Phanerozoic. Geological Society, London, Special Publications, 226(1): 73–100.
Kovalenko, V.I., Yarmolyuk, V.V., Kovach, V.P., Kotov, A.B., Kozakov, I.K., Salnikova, E.B., and Larin, A.M. 2004. Isotope provinces, mechanisms of generation and sources of the continental crust in the Central Asian mobile belt: geological and isotopic evidence. Journal of Asian Earth Sciences, 23(5): 605–627.
Küster, D., and Harms, U., 1998. Post-collisional potassic granitoids from the southern and northwestern parts of the Late Neoproterozoic East African Orogen: a review. Lithos, 45: 177–195.
Lei, W.S., Guo, J.F., Ma, J.H., Xiao, L., Li, X.C., Liu, J.F., and Li, Y., 2016. Lithogeochemistry and LA-ICP-MSZircon U-Pb Age and Its Tectonic Significance of Sujishan A-type Granite Pluton, Eastern Bogda Mountains. Geological Journal of China Universities, 22(2): 231–241 (in Chinese with English abstract).
Lei, W.S., Xu, P., Guo, J.F., Xiao, L., Li, X.C., and Li, Y., 2016. LA-ICP-MS Zircon U-Pb Dating，Geological and Geochemical Features of Sujishan Gabbro Pluton，Eastern Bogda Mountains, and Their Tectonic Significances. Geological Review, 62(2): 317–330 (in Chinese with English abstract).
Li, P.F., Sun, M., Rosenbaum, G., Cai, K.D., and Yu, Y., 2015. Structural evolution of the Irtysh Shear Zone (northwestern China) and implications for the amalgamation of arc systems in the Central Asian Orogenic Belt. Journal of Structural Geology, 80: 142–156.
Li, P.F., Sun, M., Rosenbaum, G., Jourdan, F., Li, S.Z, and Cai, K.D., 2017. Late Paleozoic closure of the Ob-Zaisan Ocean along the Irtysh shear zone (NW China): implications for arc amalgamation and oroclinal bending in the Central Asian orogenic belt. Geological Society of America Bulletin, 129: 547–569.
Li, X.H., Li, Z.X., Li, W.X., Liu, Y., Yuan, C., Wei, G., and Qi, C., 2007. U–Pb zircon, geochemical and Sr–Nd–Hf isotopic constraints on age and origin of Jurassic Iand A-type granites from central Guangdong, SE China: a major igneous event in response to foundering of a subducted flat-slab? Lithos, 96 (1): 186–204.
Li, S., Wang, T., Wilde, S.A. and Tong, Y., 2013a. Evolution, source and tectonic significance of Early Mesozoic granitoid magmatism in the Central Asian Orogenic Belt (central segment). Earth-Science Reviews, 126(0): 206–234.
Li S, Wilde S A, and Wang T. 2013b. Early Permian post-collisional high-K granitoids from Liuyuan area in southern Beishan orogen, NW China: Petrogenesis and tectonic implications. Lithos, 179: 99–119.
Li, S., Wilde, S.A., Wang, T., Xiao, W.J. and Guo, Q.Q., 2016. Latest Early Permian granitic magmatism in southern Inner Mongolia, China: Implications for the tectonic evolution of the southeastern Central Asian Orogenic Belt. Gondwana Research, 29(1): 168–180.
Li, Y.C., Yang, F.Q., Zhao, C.S., Zhang, Y., Yan, S.H., Dai, J.Z., and Xu, L.G., 2007. SHRIMP U-Pb zircon dating of the Beilekuduk pluton in Xinjiang and its geological implications. Acta Petrologica Sinica, 23(10): 2483–2492 (in Chinese with English abstract).
Liu, W, Liu, X.J., and Liu L.J., 2013. Underplating generated A– and I–type granitoids of the East Junggar from the lower and the upper oceanic crust with mixing of mafic magma: Insights from integrated zircon U–Pb ages, petrography, geochemistry and Nd–Sr–Hf isotopes. Lithos, 179: 293–319.
Long, X.P., Yuan, C., Sun, M., Safonova, I., Xiao, W.J., and Wang, Y.J., 2012. Geochemistry and U-Pb detrital zircon dating of Paleozoic graywackes in East Junggar, NW China: insights into subduction-accretion processes in the southern Central Asian Orogenic Belt. Gondwana Research, 21: 637–653.
Ludwig, K.R., 2008. Isoplot/Ex 3.70. A Geochronological Toolkit for Microsoft Excel. Berkeley Geochronological Center, Special publication No. 4.
Lustrino, M., 2005. How the delamination and detachment of lower crust can influence basaltic magmatism. Earth-Science Reviews, 72: 21–38.
Ma, R.S., Shu, L.S., and Sun, J.Q., 1997. Tectonic Evolution and Metallogeny of Eastern Tianshan Mountains. Geological Publishing House, Beijing (202 pp.).
Ma, X.H., Chen, B., Wang, C., and Yan, X.L., 2015. Early Paleozoic subduction of the Paleo-Asian Ocean: Zircon U-Pb geochronological，geochemical and Sr-Nd isotopic evidence from the Harlik pluton，Xinjiang. Acta Petrologica Sinica, 31 (1): 89–104 (in Chinese with English abstract).
Maniar, P.D., and Piccoli, P.M., 1989. Tectonic discrimination of granitoids. Geological Society of America Bulletin, 101(5): 635–643.
Mao, Q.G., Xiao, W.J., Fang, T.H., Windley, B.F., Sun, M., Ao, S.J., Zhang, J.E., and Huang, X.K., 2014. Geochronology, geochemistry and petrogenesis of Early Permian alkaline magmatism in the Eastern Tianshan: implications for tectonics of the Southern Altaids. Lithos, 190: 37–51.
Moghazi, A.M., 2003. Geochemistry and petrogenesis of a high-K calc-alkaline Dokhan Volcanic suite, South Safaga area, Egypt: the role of late Neoproterozoic crustal extension. Precambrian Research, 125: 161–178.
Pearce, J.A., Harris, N.B.W., and Tindle, A.G., 1984. Trace element discrimination diagrams for the tectonic interpretation of granitic rocks. Journal of Petrology, 25: 956– 983.
Peccerillo A, and Taylor S R. 1976. Geochemistry of eocene calc - alkaline volcanic rocks from the Kastamonu area, Northern

Turkey. Contributions to Mineralogy & Petrology, 58(1):63–81.

Qin, B., 2012. Time constraints and SHRIMP of zircon from plagioclase granite of ophiolitic in Aletunkunduo. Northwestern Geology, 45: 20–25 (in Chinese with English abstract).

Qin, K.Z., Su, B.X., Sakyi, P.A., Tang, D.M., Li, X.H., Sun, H., Xiao, Q.H., and Liu, P.P., 2011. SIMS zircon U-Pb geochronology and Sr-Nd isotopes of Ni-Cu-bearing maficultramafic intrusions in Eastern Tianshan and Beishan in correlation with flood basalts in Tarim Basin (NW China): constraints on a ca. 280 Ma mantle plume. American Journal of Science, 311: 237–260.

Qiu, J.S., Xiao, E., Hu, J., Xu, X.S., Jiang, S.Y., and Li, Z., 2008. Petrogenesis of high fractionated I-type granites in the coastal area of northeastern Fujian Province: constraints from zircon U–Pb geochronology, geochemistry, and Nd–Hf isotopes. Acta Petrologica Sinica, 24 (11): 2468–2484 (in Chinese with English abstract).

Ren, J., Niu, B., Wang, J., Jin, X., Zhao, L., and Liu, R., 2013, Advances in research of Asian geology—A summary of 1:5M International Geological Map of Asia project: Journal of Asian Earth Sciences, 72: 3–11.

Richards, J.P., 2009. Postsubduction porphyry Cu–Au and epithermal Au deposits: products of remelting of subduction-modified lithosphere. Geology, 37: 247–250.

Roberts, M.P., and Clemens, J.D., 1993. Origin of high-potassium, calc-alkaline, I-type granitoids. Geology, 21: 825–828.

Rottura, A., Bargossi, G.M., Caggianelli, A., Del Moro, A., Visonà, D., and Tranne, C.A., 1998. Origin and significance of the Permian high-K calc-alkaline magmatism in the centraleastern Southern Alps, Italy. Lithos, 45: 329–348.

Scherer, E., Münker, C., and Mezger, K., 2001. Calibration of the lutetium-hafnium clock. Science, 293(5530): 683–687.

Schott, B., and Schmeling, H., 1998. Delamination and detachment of a lithospheric root. Tectonophysics, 296: 225–247.

Seltmann, R., Konopelko, D., Biske, G., Divaev, F., and Sergeev, S., 2011. Hercynian postcollisional magmatism in the context of Paleozoic magmatic evolution of the Tien Shan orogenic belt. Journal of Asian Earth Sciences, 42: 821–838.

Sengör, A.M.C., Natal'In B.A., and Burtman, V.S., 1993. Evolution of the Altaid tectonic collage and Palaeozoic crustal growth in Eurasia. Nature, 364(6435): 299–307.

Shen, X.M., Zhang, H.X., Wang, Q., Wyman, D.A., and Yang, Y.H., 2011. Late Devonian–early Permian A–type granites in the southern Altay Range, Northwest China: Petrogenesis and implications for tectonic setting of “A2–type” granites. Journal of Asian Earth Sciences, 42 (5): 986–1007.

Shu, L.S., Wang, B., Zhu, W.B., Guo, Z.J., Charvet, J., and Zhang, Y., 2011. Timing of initiation of extension in the Tianshan, based on structural, geochemical and geochronological analyses of bimodal volcanism and olistostrome in the Bogda Shan (NW China). International Journal of Earth Sciences, 100: 1647–1663.

Song, P., Wang, T., Tong, Y., Zhang, J.J., Huang, H., and Qin, Q., 2019. Contrasting deep crustal compositions between the Altai and East Junggar orogens, SW Central Asian Orogenic Belt: Evidence from zircon Hf isotopic mapping. Lithos, 328-329: 297–311.

Song P, Tong Y, Wang T, Huang H, Zhang J J, and Huang W., 2018. Zircon U-Pb ages, genetic evolution and geological significance of Carboniferous granites in the Harlik Mountain, East Tianshan, Xinjiang. Geological Bulletin of China, 37 (5):790–804 (in Chinese with English abstract).

Song, X.Y., Chen, L.M., Deng, Y.F., and Xie, W., 2013. Syncollisional tholeiitic magmatism induced by asthenosphere upwelling owing to slab detachment at the southern margin of the Central Asian Orogenic Belt. Journal of the geological society, 170: 941–950.

Su, Y.P., Tang, H.F., and Cong, F., 2008. Zircon U-Pb age and petrogenesis of the Huangyangshan alkalinegrantie body in East Junggar, Xinjiang. Acta Mineralogica Sinica, 28(2): 117–126 (in Chinese with English abstract).

Sun, G.H., Li, J.Y., Gao, L.M., and Yang, T.N., 2005. Zircon SHRIMP U-Pb age of a dioritic pluton in the Harlik Mountain, Eastern Xinjiang, and its tectonic implication. Geological Review, 51(4): 463–469 (in Chinese with English abstract).

Sun, G.H., Li, J.Y., Zhu, Z.X., Li, Y.P., and Yang, Z.Q., 2007. Zircons SHRIMP U-Pb dating of gneissoid-biotitic granite in Harlik Mountains, Eastern of Xinjiang and it’s geological implications. Xinjiang Geology, 25(1): 4–10 (in Chinese with English abstract).

Sun, M., Long, X.P., Cai, K.D., Jiang, Y.D., Wang, B.Y., Yuan, C., Zhao, G.C., Xiao, W.J., and Wu, F.Y., 2009. Early Paleozoic ridge subduction in the Chinese Altai: Insight from the abrupt change in zircon Hf isotopic compositions. Science in China Series D: Earth Sciences, 52(9): 1345–1358.

Sun, S.S., and Mcdonough, W.F., 1989. Chemical and isotopic systematics of oceanic basalts: Implications for mantle composition and processes. Geological Society of London Special Publications, 42(1):313–345.

Sylvester P J., 1989. Post- collisional alkaline granites. The Journal of Geology, 97(3): 261–280.

Tao, J., Li, W., Li, X., and Cen, T., 2013. Petrogenesis of early Yanshanian highly evolved granites in the Longyuanba area, southern Jiangxi Province: evidence from zircon U–Pb dating, Hf–O isotope and whole-rock geochemistry. Science China Earth Sciences, 56 (6): 922–939.

Tong, Y., Wang, T., Jahn, B.M., Sun, M., Hong, D.W., and Gao, J.F., 2014. Post–accretionary permian granitoids in the Chinese Altai orogen: Geochronology, petrogenesis and tectonic implications. American Journal of Science, 314: 80–109.

Tong, Y., Wang, T., Siebel W., Hong, D.W., and Sun, M., 2012. Recognition of early Carboniferous alkaline granite in the southern Altai orogen: post–orogenic processes constrained by U–Pb zircon ages, Nd isotopes, and geochemical data. International Journal of Earth Sciences, 101(4): 937–950.

Wang, B., Cluzel, D., Jahn, B.-M., Shu, L., Chen, Y., Zhai, Y., Branquet, Y., Barbanson, L., and Sizaret, S., 2014. Late Paleozoic pre- and syn-kinematic plutons of the Kangguer–Huangshan Shear zone: inference on the tectonic evolution of the eastern Chinese north Tianshan. American Journal of Science, 314: 43–79.

Wang, B.Y., Jiang, C.Y., Li, Y.J., Wu, H.E., Xia, Z.D., and Lu, R.H., 2009. Geochemistry and tectonic implications of Karamaili ophiolite in East Junggar of Xinjiang. Journal of Mineralogy and Petrology, 29: 74–82 (in Chinese with English abstract).

Wang, C.S., Gu, L.X., Zhang, Z.Z., Wu, C.Z., Tang, J.H., and Tang, X.Q., 2009. Petrogenesis and geological implications of the Permian high-K calc-alkaline granites in Harlik Mountains of eastern Tianshan, NW China. Acta Petrologica Sinica, 25 (6): 1499–1511 (in Chinese with English abstract).

Wang, C.S., Zhang, Z.Z., Gu, L.X., Wu, C.Z., Tang, J.H., Li, Z.H., Feng, H., and Lei, R.X., 2010. Zircon geochronology and geochemical characteristics of the Permian granitic complex at Yiwu, eastern Tianshan: Their tectonic significance. Acta Petrologica Sinica, 26(4): 1045-1058 (in Chinese with English abstract).

Wang, Y.H., Zhang, F.F., Liu, J.J., Xue, C.J., Wang, J.P., Liu, B., and Lu, W.W., 2015. Petrogenesis of granites in Baishan molybdenum deposit, eastern Tianshan, Xinjiang: Zircon U-Pb geochronology, geochemistry, and Hf isotope constraints. Acta Petrologica Sinica, 31(7): 1962–1976 (in Chinese with English abstract).

Whalen, J.B., Currie, K.L., and Chappell, B.W., 1987. A-type granites: geochemical characteristics, discrimination and petrogenesis. Contributions to Mineralogy and Petrology, 95 (4): 407–419.

Wilhem, C., Windley, B.F., and Stampfli, G.M., 2012. The Altaids of Central Asia: A tectonic and evolutionary innovative review. Earth–Science Reviews, 113(3–4): 303–341.

Windley, B.F., Kröner, A., Guo, J.H., Qu, G.S., Li, Y.Y., and Zhang, C., 2002. Neoproterozoic to Paleozoic Geology of the Altai Orogen, NW China: New Zircon Age Data and Tectonic

Evolution. The Journal of Geology, 110(6): 719–737.
Windley, B.F., Alexeiev, D., Xiao, W.J., Kroener, A., and Badarch, G., 2007. Tectonic models for accretion of the Central Asian Orogenic Belt. Journal of the Geological Society, 164(1): 31–47.
Wu, F.Y., Jahn, B.M., Wilde, S.A., Lo, C.H., Yui, T.F., Lin, Q., Ge, W.C., and Sun, D.Y., 2003. Highly fractionated I-type granites in NE China (II): isotopic geochemistry and implications for crustal growth in the Phanerozoic. Lithos, 67 (3-4): 191–204.
Wu, F.Y., Li, X.H., Zheng, Y.F., and Gao, S., 2007. Lu–Hf isotopic systematics and their applications in petrology. Acta Petrologica Sinica, 23(2): 185–220 (in Chinese with English abstract).
Xiao, W.J., Zhang, L.C., Qin, K.Z., Sun, S., and Li, J.L., 2004. Paleozoic accretionary and collisional tectonics of the eastern Tianshan (China): implications for the continental growth of central Asia. American Journal of Science, 304: 370–395.
Xiao, W.J., Han, C.M., Yuan, C., Sun, M., Lin, S.F., Chen, H.L., Li, Z.L., Li, J.L., and Sun, S., 2008. Middle Cambrian to Permian subduction-related accretionary orogenesis of North Xinjiang, NW China: implications for the tectonic evolution of Central Asia. Journal of Asian Earth Sciences, 32: 102–117.
Xiao, W.J., Windley, B.F., Yuan, C., Sun, M., Han, C.M., Lin, S.F., Chen, H.L., Yan, Q.R., Liu, D.Y., Qin, K.Z., Li, J.L., and Sun, S., 2009. Paleozoic multiple subduction–accretion processes of the southern Altaids. American Journal of Science, 309: 221–270.
Xiao, W.J., Mao, Q.G., Windley, B.F., Han, C.M., Qu, J.F., Zhang, J.E., Ao, S.J., Guo, Q.Q., Cleven, N.R., Lin, S.F., Shan, Y.H., and Li, J.L., 2010. Paleozoic multiple accretionary and collisional processes of the Beishan orogenic collage. American Journal of Science, 310: 1553–1594.
Xiao, Y., Zhang, H.F., Shi, Ji'an, Su, B.X., Sakyi, P.A., Lu, X.C., Hu, Y., and Zhang, Z., 2011. Late Paleozoic magmatic record of East Junggar, NW China and its significance: Implication from zircon U–Pb dating and Hf isotope. Gondwana Research, 20 (2-3): 532–542.
Xu, Q.Q., Ji, J.Q., Zhao, L., Gong, J.F., Zhou, J., He, G.Q., Zhong, D.L., Wang, J.D., and Griffiths, L., 2013. Tectonic evolution and continental crust growth of Northern Xinjiang in northwestern China: Remnant ocean model. Earth-Science Reviews, 126: 178-205.
Xu, X.W., Jiang, N., Li, X.H., Qu, X., Yang, Y.H., Mao, Q., Wu, Q., Zhang, Y., and Dong, L.H., 2013. Tectonic evolution of the East Junggar terrane: Evidence from the Taheir tectonic window, Xinjiang, China. Gondwana Research, 24(2): 578–600.
Xu, X.W., Jiang, N., Li, X.H., Wu, C., Qu, X., Zhou, G., and Dong, L.H., 2015. Spatial–temporal framework for the closure of the Junggar Ocean in central Asia: new SIMS zircon U–Pb ages of the ophiolitic mélange and collisional igneous rocks in the Zhifang area, East Junggar. Journal of Asian Earth Sciences, 111: 470–491.
Yang, G.X., Li, Y.J., Wu, H.E., Si, G.H., Jin, Z., and Zhang, Y.Z., 2009. LA-ICP-MS zircon U-Pb dating of the Huangyangshan pluton and its enclaves from Kalamaili area eastern Junggar, Xinjiang, and geological implications. Acta Petrolocia Sinica, 25(12): 3197-3207 (in Chinese with English abstract).
Yang, G.X., Li, Y.J., Si, G.H., Wu, H.E., Zhang, Y.Z., and Jin, Z., 2010. LA-ICP-MS zircon U-Pb dating of Kubusunan granodiorite and the enclaves from Kalamaili Area in eastern Junggar, Xinjiang, and its geological implications. Earth Science-Journal of China University of Geosciences, 35(4): 597-610 (in Chinese with English abstract).
Yang, G.X., Li, Y.J., Wu, H.E., Zhong, X., Yang, B.K., Yan, C.X., Yan, J., and Si, G.H., 2011. Geochronological and geochemical constrains on petrogenesis of the Huangyangshan A-type granite from the East Junggar, Xinjiang, NW China. Journal of Asian Earth Sciences, 40(3): 722–736.
Yang, J.H., Sun, J.F., Zhang, J.H., and Wilde, S.A., 2012. Petrogenesis of Late Triassic intrusive rocks in the northern Liaodong Peninsula related to decratonization of the North China Craton: zircon U–Pb age and Hf–O isotope evidence. Lithos, 153: 108–128.
Yuan, C., Sun, M., Xiao, W.J., Li, X.H., Chen, H.L., Lin, S.F., Xia, X.P., and Long, X.P., 2007. Accretionary orogenesis of the Chinese Altai: Insights from Paleozoic granitoids. Chemical Geology, 242(1): 22–39.
Yuan, C., Sun, M., Wilde, S., Xiao, W.J., Xu, Y.G., Long, X.P., and Zhao, G.C., 2010. Post-collisional plutons in the Balikun area, East Chinese Tianshan: evolving magmatism in response to extension and slab break-off. Lithos, 119: 269–288.
Zhang, C., Liu, D.D., Luo, Q., Liu, L.F., Zhang, Y.Z., Zhu, D.Y., Wang, P.F., and Dai, Q.Q., 2018. An evolving tectonic environment of Late Carboniferous to Early Permian granitic plutons in the Chinese Altai and Eastern Junggar terranes, Central Asian Orogenic Belt, NW China. Journal of Asian Earth Sciences, 159: 185–208.
Zhang, Y., Liang, G.L., Qu, X., Du, S.J., Wu, Q., Zhang, Z.F., Dong, L.H., and Xu, X.W., 2010. Evidence of U-Pb age and Hf isotope of zircons for Early Paleozoic magmatism in the Qiongheba arc，East Junggar. Acta Petrologica Sinica, 26(8): 2389–2398 (in Chinese with English abstract).
Zhou, M.F., Michael Lesher, C., Yang, Z.X., Li, J.W., and Sun, M., 2004. Geochemistry and petrogenesis of 270 Ma Ni-Cu-(PGE) sulfide-bearing mafic intrusions in the Huangshan district, Eastern Xinjiang, Northwest China: implications for the tectonic evolution of the Central Asian orogenic belt. Chemical Geology, 209: 233–257.
Zhou, T.F., Yuan, F., Zhang, D.Y., Fan, Y., Liu, S., Peng, M.X., and Zhang, J.D., 2010. Geochronology, tectonic setting and mineralization of granitoids in Jueluotage area, eastern Tianshan, Xinjiang. Acta Petrologica Sinica, 26: 478–502 (in Chinese with English abstract).
Zhu, D.C., Mo, X.X., Wang, L.Q., Zhao, Z.D., Niu, Y.L., Zhou, C.Y., and Yang, Y.H., 2009. Petrogenesis of highly fractionated I-type granites in the Zayu area of eastern Gangdese, Tibet: constraints from zircon U-Pb geochronology, geochemistry and Sr-Nd-Hf isotopes. Science in China (Series D: Earth Sciences), 52 (9): 1223–1239.

About the first author

SONG Peng, male, born in 1988 in Jinan City, Shandong Province; doctor; graduated from Chinese Academy of Geological Sciences; postdoctor of Institute of Geology, Chinese Academy of Geological Sciences. He is now interested in the study on granitoid, tectonics and continental growth. Email: songpengyx@foxmail.com; phone: 010-68999732, 15010282102.

About the corresponding author

WANG Tao, male, born in 1959 in Shihezi City, Xinjiang Province; doctor; graduated from Northwest University; researcher of Institute of Geology, Chinese Academy of Geological Sciences. He is now interested in the study on granitoid and tectonics. Email: taowang@cags.ac.cn.